Atoms trapped by a spin-dependent optical lattice potential: Realization of a ground-state quantum rotor

Igor Kuzmenko,[1,2] Tetyana Kuzmenko,[1] Y. Avishai,[1,4] and Y. B. Band[1,2,3,4]

[1]*Department of Physics, Ben-Gurion University of the Negev, Beer-Sheva 84105, Israel*

[2]*Department of Chemistry, Ben-Gurion University of the Negev, Beer-Sheva 84105, Israel*

[3]*Department of Electro-Optics, Ben-Gurion University of the Negev, Beer-Sheva 84105, Israel*

[4]*The Ilse Katz Center for Nano-Science, Ben-Gurion University of the Negev, Beer-Sheva 84105, Israel*

(Received 16 March 2019; published 19 September 2019)

In a cold atom gas subject to a two-dimensional spin-dependent optical lattice potential with hexagonal symmetry, trapped atoms execute circular motion around the potential minima. Such atoms are elementary quantum rotors. The theory of such quantum rotors is developed. Wave functions, energies, and degeneracies are determined for both bosonic and fermionic atoms, and magnetic dipole transitions between quantum rotor states are elucidated. Quantum rotors in optical lattices with precisely one atom per unit cell can be used as extremely high sensitivity rotation sensors, accelerometers, and magnetometers.

DOI: 10.1103/PhysRevA.100.033415

I. INTRODUCTION

A quantum-mechanical system in which the motion of a particle is constrained to a circular ring (or a multidimensional spherical shell) is an elementary quantum rotor (QR) [1]. References [1,2] state that "elementary QRs do not exist in nature." Here we consider both bosonic and fermionic cold atoms subject to a two-dimensional (2D) spin-dependent optical lattice potential (SDOLP) of hexagonal symmetry, and show that the trapped atoms behave as elementary QRs. We demonstrate that QRs with *singly occupied sites* (so deleterious spin-relaxation effects are thereby suppressed) can be used as high accuracy rotation sensors, accelerometers, and magnetometers.

Quantum rotors have been formed using Laguerre-Gaussian beams [3,4]; e.g., see Refs. [5,6]. However, these references mostly considered the many-body prosperities of cold atomic clouds in these beams and were not focused on *elementary* quantum rotors. In contrast, our interest is in singly occupied sites of SDOLPs so that interactions between QR atoms are suppressed. Hence the systems we consider are elementary QRs. Moreover, here we show that these QRs can be used as high accuracy rotation sensors, accelerometers, and magnetometers, and this not considered in Refs. [5,6].

The outline of the paper is as follows. In Sec. II we present the model of the quantum rotors in the SDOLP. Section II A presents the 2D isotropic approximation for the SDOLP, and Sec. II B discusses the exotic properties of these QRs. The stimulated Raman spectroscopy used to probe the QRs is considered in Sec. III, and in Sec. III A we focus on far-off-resonance Raman transitions between the ground-state levels $n = 0, \zeta = 1/2$ and $n = 0, \zeta = -1/2$. Section IV explains how to use the QRs in the SDOLP with singly occupied sites as a high precision magnetometer, Sec. V discusses the use of these QRs as rotation sensors, and Sec. VI discusses the use of these QRs as accelerometers. In Sec. VII we provide estimates of the accuracy of measurements of rotation, acceleration, and magnetic field using QRs, and in Sec. VIII we calculate the uncertainty due to shot noise in the Stokes and pump pulses. Finally, a summary and conclusion are presented in Sec. IX. In order to clarify some of the ideas presented in the main text, we provide a number of Appendices with background material and further details that substantiate the material presented in the main text. Specifically, Appendix A provides additional details regarding SDOLP, and Appendix B presents further details on the isotropic approximation for the potential near its minima. The QR areal probability density is studied in Appendix C. Appendix D provides a semiclassical description of the quantum QR. Finally, Appendix E discusses a method of distinguishing between the effects of rotation, acceleration, and external magnetic field on the QR.

II. MODEL

Consider alkali atoms trapped in the x-y plane by a SDOLP [7–13]. As shown schematically in Fig. 1, an optical lattice potential with hexagonal symmetry [14] is formed by six coherent laser beams of wavelength $\lambda_0 = \frac{2\pi}{q_0}$ and wave vectors $\mathbf{q}_n = -q_0(\cos(n\pi/3), \sin(n\pi/3))$ with $n = 1, 2, 3, \ldots, 6$. The resultant electric field is $\mathbf{E}(\mathbf{r}, t) = [\mathbf{E}(\mathbf{r})e^{-i\omega_0 t} + \text{c.c.}]/2$ with amplitude E_0 and space dependent part

$$\mathbf{E}(\mathbf{r}) = E_0 \sum_{n=1}^{6} \boldsymbol{\xi}_n e^{i\mathbf{q}_n \mathbf{r}}, \tag{1}$$

where the polarization vectors $\boldsymbol{\xi}_n$ are

$$\boldsymbol{\xi}_n = \left\{ \sqrt{1-\beta^2}\mathbf{e}_z + \frac{\beta}{q_0}\mathbf{q}_n \times \mathbf{e}_z \right\}. \tag{2}$$

The electric field (1) is a linear combination of standing waves with in-plane and out-of-plane linear polarization with

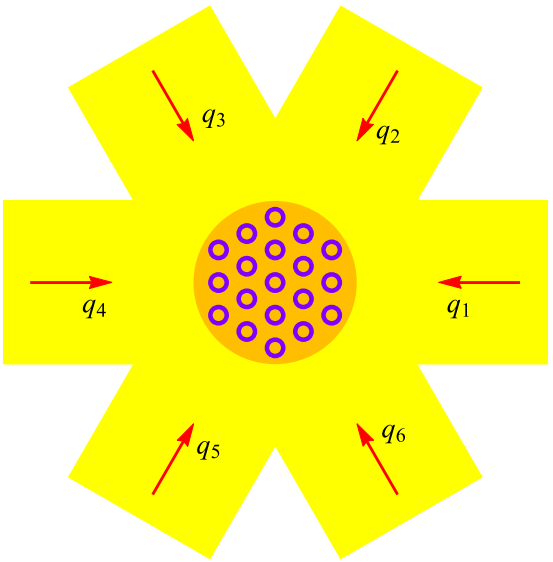

FIG. 1. Laser beams (yellow) with wave vectors $\mathbf{q}_n$ in the x-y plane generate an optical lattice potential with hexagonal symmetry. The orange disk in the center shows the physical region in which the optical lattice is located.

real mixing parameter $0 < \beta < 1$ (in what follows we take $\beta = 1/\sqrt{2}$). It generates an effective SDOLP experienced by the atoms.

The quantum states of the trapped atoms are described by the electronic angular momentum J, the nuclear spin I, and the total internal atomic angular momentum quantum number F ($\mathbf{F} = \mathbf{J} + \mathbf{I}$). As we shall see, atoms with $F \neq 0$ rotate in a closed circular ring in the x-y plane around local minima of the scalar optical lattice potential. The corresponding orbital angular momentum operator is denoted by $\boldsymbol{\ell}$. The projections of $\mathbf{F}$, $\boldsymbol{\ell}$, and the total angular momentum of the QR, $\boldsymbol{\mathcal{L}} = \mathbf{F} + \boldsymbol{\ell}$, on the z axis are f, m, and $\zeta = f + m$, respectively. For bosonic (fermionic) atoms ζ is an integer (half integer). Generically, the optical potential is not diagonal in F or in f [9] (for further details see Appendix A). However, when the off-diagonal elements in F are much smaller than the atomic hyperfine splitting, the mixing of atomic energy levels with different quantum numbers F can be neglected.

For $J = 1/2$, the optical lattice Stark interaction Hamiltonian is calculated as the second-order ac Stark shift. In the hyperfine basis it takes the form [9,15] (see also Appendix A2 for details)

$$H_{\text{Stark}}(\mathbf{r}) = V(\mathbf{r})1 - \mathbf{B}(\mathbf{r}) \cdot \mathbf{F}, \tag{3}$$

where $\mathbf{1}$ is the $(2F + 1) \times (2F + 1)$ unity matrix. The scalar optical potential $V(\mathbf{r})$ and fictitious magnetic field $\mathbf{B}(\mathbf{r})$ [16] (which has units of energy) are

$$V(\mathbf{r}) = -\frac{\alpha_0(\omega_0)}{4}\mathbf{E}^*(\mathbf{r}) \cdot \mathbf{E}(\mathbf{r}), \tag{4a}$$

$$\mathbf{B}(\mathbf{r}) = \frac{i\alpha_1(\omega_0)}{4(2I+1)}[\mathbf{E}^*(\mathbf{r}) \times \mathbf{E}(\mathbf{r})], \tag{4b}$$

TABLE I. Recoil temperatures $T_0 = \mathcal{E}_0/k_B = \hbar^2 q_0^2/(2Mk_B)$ for some atoms.

Fermions		Bosons	
Atom	T_0 (μK)	Atom	T_0 (μK)
^{2}H	321.7	^{7}Li	3.031
^{6}Li	3.536	^{23}Na	1.197
^{40}K	0.404	^{39}K	0.414

where $\alpha_0(\omega_0)$ and $\alpha_1(\omega_0)$ are scalar and vector polarizabilities of the atom [9,17]. For $J > 1/2$, a tensor term is also present in Eq. (A14) (see Ref. [9]).

Both $V(\mathbf{r})$ and $\mathbf{B}(\mathbf{r})$ are periodic, $V(\mathbf{r}) = V(\mathbf{r} + m_1\mathbf{a}_1 + m_2\mathbf{a}_2)$ and $\mathbf{B}(\mathbf{r}) = \mathbf{B}(\mathbf{r} + m_1\mathbf{a}_1 + m_2\mathbf{a}_2)$, where m_1 and m_2 are integers and the lattice vectors are $\mathbf{a}_j = \lambda_0(\mathbf{e}_x \sin\theta_j + \mathbf{e}_y \cos\theta_j)$, where $j = 1$ and 2 and $\theta_j = (-1)^j\pi/3$. $V(\mathbf{r})$ has minima at $\mathbf{r}_{\min} = m_1\mathbf{a}_1 + m_2\mathbf{a}_2$. $\mathbf{B}(\mathbf{r})$ is a pseudovector [9], and changes sign under time reversal (but the QR Hamiltonian is time-reversal invariant). $V(\mathbf{r})$ and $\mathbf{B}(\mathbf{r})$ are plotted versus $\mathbf{r}$ in Fig. 7 in Appendix A2.

The loss of atoms from the near-detuned SDOLP due to excited-state spontaneous emission can be phenomenologically taken into account by including an imaginary contribution to the energy denominator of the second-order ac Stark shift [see Eq. (A7) of Appendix A]. The loss rate is given by

$$\Gamma(\mathbf{r}) = \frac{V(\mathbf{r})\gamma_e}{2\hbar\Delta}, \tag{5}$$

where Δ is the detuning of the optical frequency from resonance and γ_e is the inverse lifetime of the excited electronic state. As we shall soon see, the loss rate $\Gamma(\mathbf{r})$ will affect the accuracy of the sensors considered below.

Candidates for observing QR states include the fermions ^{2}H, ^{6}Li, and ^{40}K and the bosons ^{7}Li, ^{23}Na, ^{39}K, ^{85}Rb, and ^{87}Rb. All of these have nonvanishing F in their ground electronic state [18]. Recoil temperatures $T_0 = \mathcal{E}_0/k_B$ for some of these fermionic and bosonic species are listed in Table I.

A. 2D isotropic approximation

We assume hereafter that the depth of $V(\mathbf{r})$ at the minimum positions exceeds the recoil energy $\mathcal{E}_0 = \hbar^2 q_0^2/(2M)$, where M is the atomic mass, and the low-energy atomic states are trapped and localized near these minima. For hexagonal symmetry, the scalar potential near the minimum at $\mathbf{r} = (0, 0)$ is well approximated by $V(\mathbf{r}) \approx \tilde{V}(r)$, where

$$\tilde{V}(r) = -\frac{V_0}{6}\left[2 + 3J_0\left(\frac{2\pi r}{\lambda_0}\right) + J_0\left(\frac{2\sqrt{3}\pi r}{\lambda_0}\right)\right], \tag{6}$$

and $V_0 = \frac{9}{2}\alpha_0(\omega_0)E_0^2$. The fictitious magnetic field near this minimum can be approximated by $\mathbf{B}(r) \approx \tilde{B}(r)\mathbf{e}_r$ where

$$\tilde{B}(r) = \frac{B_0}{3(2I+1)}\left[J_1\left(\frac{2\pi r}{\lambda_0}\right) + J_1\left(\frac{4\pi r}{\lambda_0}\right) + \sqrt{3}J_1\left(\frac{2\sqrt{3}\pi r}{\lambda_0}\right)\right]. \tag{7}$$

Here $B_0 = \frac{9}{2}\alpha_1(\omega_0)E_0^2$, $J_n(\rho)$ is the Bessel function of order n, and the unit vector $\mathbf{e}_r \equiv \hat{\mathbf{r}}$. The dependence of V_0 and B_0 on the detuning of ω_0 from resonance is discussed in Appendix A2.

The (fictitious) Zeeman interaction $\mathbf{B}(\mathbf{r}) \cdot \mathbf{F}$ is proportional to $F_r = \mathbf{F} \cdot \mathbf{e}_r$ [since $\mathbf{B}(\mathbf{r})$ is radial] and does not commute with the operators F_z or ℓ_z $(= -i\partial_\phi)$, but commutes with $\mathcal{L}_z = F_z + \ell_z$. Hence, f and m are not individually good quantum numbers of the total Hamiltonian but ζ, the eigenvalue of the operator $\mathcal{L}_z$, is. The wave functions $\Psi_{n,\zeta}(\mathbf{r})$ and energy levels $\epsilon_{n,\zeta}$ of the trapped atoms satisfy the Schrödinger equation [19]

$$\left[-\frac{\hbar^2\nabla^2}{2M} + \tilde{V}(r) - \tilde{B}(r)F_r - \epsilon_{n,\zeta}\right]\Psi_{n,\zeta}(\mathbf{r}) = 0, \tag{8}$$

and the functions $\Psi_{n,\zeta}(\mathbf{r})$ can be expanded as follows:

$$\Psi_{n,\zeta}(\mathbf{r}) = \frac{1}{\sqrt{2\pi r}}\sum_\sigma \psi_{n,\zeta,\sigma}(r)e^{i\zeta\phi}\chi_\sigma(\phi). \tag{9}$$

Here $\chi_\sigma(\phi)$ are spinor eigenfunctions of F_r, i.e., $F_r\chi_\sigma(\phi) = \sigma\chi_\sigma(\phi)$ (σ should not be confused with f, the eigenvalue of F_z).

Explicitly, for $F = 1/2$ (e.g., ^{6}Li), $\sigma = \pm 1/2$, and $\chi_\sigma(\phi)$ is given by

$$\chi_{\sigma=\pm1/2}(\phi) = \frac{1}{\sqrt{2}}\left\{e^{-\frac{i\phi}{2}}\chi_\uparrow^{(z)} \pm e^{\frac{i\phi}{2}}\chi_\downarrow^{(z)}\right\},$$

where $\chi_f^{(z)}$ are eigenfunctions of F_z with eigenvalues f. Inserting the expansion (9) into Eq. (8) we obtain

$$\left[-\frac{\hbar^2}{2M}\frac{\partial^2}{\partial r^2} + \tilde{V}(r) - \frac{1}{2}\tilde{B}(r) + \zeta^2 C(r) - \epsilon_{n,\zeta}\right]\psi_{n,\zeta,1/2}(r) = \zeta C(r)\psi_{n,\zeta,-1/2}(r), \tag{10a}$$

$$\left[-\frac{\hbar^2}{2M}\frac{\partial^2}{\partial r^2} + \tilde{V}(r) + \frac{1}{2}\tilde{B}(r) + \zeta^2 C(r) - \epsilon_{n,\zeta}\right]\psi_{n,\zeta,-1/2}(r) = \zeta C(r)\psi_{n,\zeta,1/2}(r), \tag{10b}$$

where the off-diagonal spin-flipped terms are proportional to $C(r) = \hbar^2/(2Mr^2)$. The numerical calculations presented below will be for the fermionic case with $F = 1/2$, assuming that $V_0, |B_0| \gg \mathcal{E}_0$. The inequality $V_0 \gg \mathcal{E}_0$ means that the potential wells are deep and the tunneling probability of the atoms between the wells is small. The wave functions and the eigenenergies $\epsilon_{n,\zeta}$ of the trapped atoms are computed by solving the Sturm-Liouville system of equations (10) with $V_0 = 100\mathcal{E}_0$, $B_0 = 180\mathcal{E}_0$. The resulting energies $\epsilon_{n,\zeta}$ are shown in Fig. 2. For the fermionic case, all the energy levels are twofold degenerate, $\epsilon_{n,\zeta} = \epsilon_{n,-\zeta}$. The off-diagonal terms $\zeta C(r)\psi_{n,\zeta,\bar{\sigma}}(r)$ (where $\bar{\sigma} = -\sigma$) in (10) are a weak perturbation to the ground-state energy level, but not so for the excited states. The degenerate fermionic ground state has quantum numbers $(n, \zeta) = (0, \pm 1/2)$, and energy $\epsilon_{0,\pm1/2} = -99.196\,\mathcal{E}_0$. The lowest-energy excited states are orbital excitations with quantum numbers $(n, \zeta) = (0, \pm 3/2)$ and radial excitations with quantum numbers $(1, \pm 1/2)$ (see Fig. 2). The corresponding excitation energies are

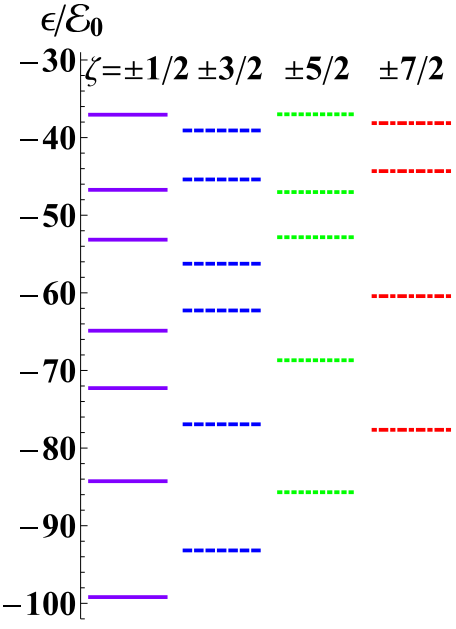

FIG. 2. Fermionic QR energy levels for $F = 1/2$ with $V_0 = 100\,\mathcal{E}_0$ and $B_0 = 180\,\mathcal{E}_0$. The solid purple, dashed blue, dotted green, and dot-dashed red lines correspond to energy levels with $\zeta = \pm 1/2$, $\pm 3/2$, $\pm 5/2$, and $\pm 7/2$. The energy levels with $n = 0, 1, \ldots$, go from bottom to top.

$$\epsilon_{0,\frac{3}{2}} - \epsilon_{0,\frac{1}{2}} = 6.011\mathcal{E}_0, \tag{11a}$$

$$\epsilon_{1,\frac{1}{2}} - \epsilon_{0,\frac{1}{2}} = 14.93\mathcal{E}_0. \tag{11b}$$

For temperatures $T \ll T_{\rm orbit} \equiv (\epsilon_{0,\frac{3}{2}} - \epsilon_{0,\frac{1}{2}})/k_B$, the trapped atoms are in their ground state. $T_{\rm orbit}$ is of order T_0 [see Eq. (11a)].

The ground-state areal probability density,

$$\rho(r) = |\Psi_{0,1/2}(\mathbf{r})|^2, \tag{12}$$

depends only on r and not on ϕ since the optical lattice potential is nearly isotropic about the potential minima. $\rho(r)$ has a maximum at $r = r_0 = 0.068\,\lambda_0$, and decays with $|r - r_0|$, as shown in Fig. 3. Thus, the atom is confined near a circular ring of radius r_0 (hence it is a QR [1]). $\rho(r)$ vanishes linearly with r as $r \to 0$. The QR ground-state density can be observed as described in Ref. [20].

B. Exotic properties of the QR state

The following exotic expectation values are obtained for the QR:

$$\langle n, \zeta|\ell_z|n, \zeta\rangle = \zeta - \langle n, \zeta|F_z|n, \zeta\rangle, \tag{13}$$

$$\langle n, \zeta|\ell_z^2|n, \zeta\rangle = \zeta^2 - \langle n, \zeta|2\zeta F_z - F_z^2|n, \zeta\rangle. \tag{14}$$

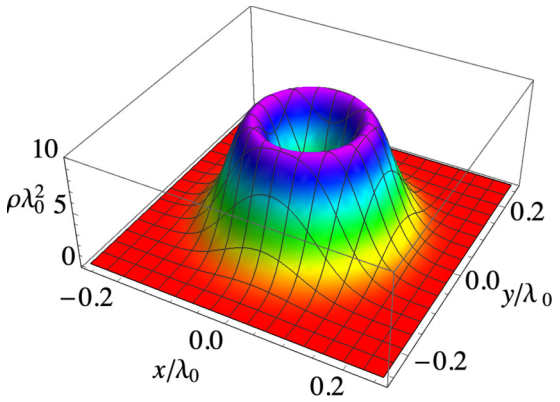

FIG. 3. The ground-state areal probability density (12) vs $\mathbf{r} = (x, y)$ for a $F = 1/2$ fermionic atom.

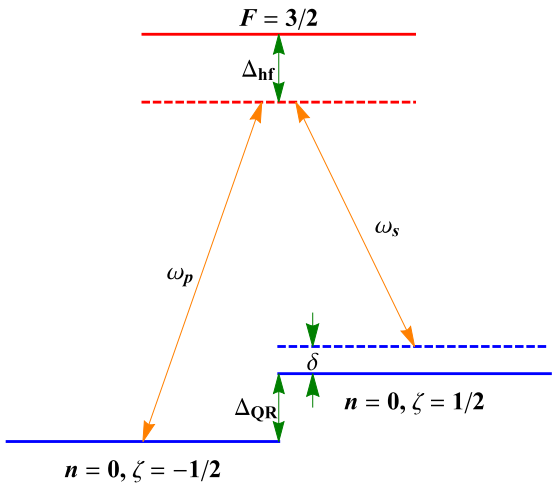

FIG. 4. Schematic representation of the energy levels and photon energies for the far-off-resonance Raman transition between the split QR ground states.

Recall that $\Psi_{n,\zeta}(\mathbf{r}) = \langle \mathbf{r}|n, \zeta\rangle$ are eigenfunctions of $\mathcal{L}_z = \ell_z + F_z$ with eigenvalue ζ; however, $\Psi_{n,\zeta}(\mathbf{r})$ is not an eigenfunction of F_z or F_z^2, and $\langle n, \zeta|F_z^2|n, \zeta\rangle \neq 0$.

For fermionic or bosonic QRs, the wave functions $\Psi_{n,\zeta}(\mathbf{r})$ in Eq. (9) are expressed as sums of products of spatial wave functions $\psi_{n,\zeta,\sigma}(r)e^{i\zeta\phi}$ and spin-wave functions $\chi_\sigma(\phi)$. They have unusual symmetry relations under rotation through an angle 2π around the z axis. The angular part of the spatial wave function satisfies $e^{i\zeta(\phi+2\pi)} = \pm e^{i\zeta\phi}$ (upper sign for bosons and lower sign for fermions), and the spin-wave function satisfies $e^{2\pi i\mathcal{L}_z}\chi_\sigma(\phi) = \chi_\sigma(\phi)$.

For bosonic QRs, ζ and σ are integers, so the angular parts of the spatial wave functions, $e^{i\zeta\phi}$, and the spin-wave functions satisfy the properties $e^{i\zeta(\phi+2\pi)} = e^{i\zeta\phi}$ and $e^{2\pi i\mathcal{L}_z}\chi_\sigma(\phi) = \chi_\sigma(\phi)$. The nondegenerate ground state $|n = 0, \zeta = 0\rangle$ is such that $\langle 0, 0|F_z|0, 0\rangle = 0$, but $\langle 0, 0|F_z^2|0, 0\rangle \neq 0$, and therefore $\langle 0, 0|\ell_z^2|0, 0\rangle \neq 0$. The spin-excited QR states have $\zeta \neq 0$ and are doubly degenerate [see Eq. (1.23) in Ref. [1]]. All states have an areal density which vanishes at $r = 0$.

For fermionic QRs, ζ and σ are half integers, and all states (including the ground state) are doubly degenerate. The ground state has $n = 0$ and $\zeta = \pm 1/2$, and is an *exotic QR* since it is *twofold degenerate* with finite orbital angular momentum. The expectation values of ℓ_z and ℓ_z^2 are nonzero. For $F = 1/2$, $\langle n, \zeta|\ell_z|n, \zeta\rangle = \frac{\zeta}{2} - \beta_{n,\zeta}^z$, and $\langle n, \zeta|\ell_z^2|n, \zeta\rangle = \frac{1}{2} - |\beta_{n,\zeta}^z|$, where

$$\beta_{n,\zeta}^z = \frac{1}{2}\sum_\sigma \int \psi_{n,\zeta,\sigma}\psi_{n,\zeta,-\sigma}\,dr. \tag{15}$$

A striking consequence of the above analysis, which will be substantiated below, is that ground-state QRs with precisely one atom per site can serve as rotation sensors, accelerometers, and magnetometers. For these applications and for the study of QRs in general, radio wave spectroscopy and Raman spectroscopy are valuable tools.

III. QR STIMULATED RAMAN SPECTROSCOPY

Consider Raman transitions between the QR states $|n = 0, \zeta = 1/2\rangle$ and $|n = 0, \zeta = -1/2\rangle$ that are split by an energy $\hbar\Delta_{QR}$ due to the presence of an external magnetic field, and/or rotation, and/or in-plane acceleration. We explicitly consider far-off-resonance radio wave transitions that are red detuned from the $F = 3/2$ atomic hyperfine state by a large detuning Δ_{hf}, $\Delta_{hf} < 0$, and $|\Delta_{hf}| \gg \gamma_{hf}$, where γ_{hf} is the decay rate of the $F = 3/2$ hyperfine state (see Fig. 4 in Sec. III A). Far-off-resonance stimulated Raman scattering can be treated as a two-level system with a generalized Raman Rabi frequency, $\Omega_g = \frac{\Omega_p\Omega_s}{\Delta_{hf}}$. The pump laser has frequency ω_p and Rabi frequency Ω_p and takes the system up from the lower of the two QR states to a virtual intermediate state, and the Stokes radiation has frequency ω_s and Rabi frequency Ω_s and takes the system down from the virtual intermediate state to the upper of the two QR states. Let $\delta = \omega_p - \omega_s - \Delta_{QR}$ be the detuning from Raman resonance. The dressed-state [21] complex Hamiltonian in the two-level $|n = 0, \zeta = \pm 1/2\rangle$ manifold, which incorporates decay of the QR states, can be written as [22]

$$H_{\text{Raman}} = \hbar\begin{pmatrix} 0 - i\Gamma_{0,1/2}/2 & \Omega_g/2 \\ \Omega_g/2 & \delta - i\Gamma_{0,-1/2}/2 \end{pmatrix}. \tag{16}$$

Symmetry requires that the loss rates $\Gamma_{0,\pm 1/2}$ of the two QR states due to loss of atoms from the SDOLP be equal, $\Gamma_{0,1/2} = \Gamma_{0,-1/2}$; they are given by (see Sec. III A below for details)

$$\Gamma_{0,1/2} = \frac{\gamma_e}{2\hbar\Delta}\sum_\sigma\left\{\int \tilde{V}(r)\psi_{0,1/2,\sigma}^2(r)dr + \frac{\text{sign}(\sigma)}{2}\int \tilde{B}(r)\psi_{0,1/2,\sigma}^2(r)dr\right\}. \tag{17}$$

Here Δ is the detuning of the laser beams generating the SDOLP and γ_e is the spontaneous emission decay rate of the $^2P_{3/2}$ excited state. The difference of the eigenvalues of H_{Raman}, $\tilde{\Omega} = \sqrt{\delta^2 + \Omega_g^2}$, is independent of $\Gamma_{0,1/2}$.

A. Far-off-resonance Raman transitions between $n = 0, \zeta = 1/2$ and $n = 0, \zeta = -1/2$

Far-off-resonance Raman transitions between the QR states $|n = 0, \zeta = 1/2\rangle$ and $|n = 0, \zeta = -1/2\rangle$ that are split by an energy $\hbar\Delta_{QR}$ are described by the model Hamiltonian

(16). Here we derive Hamiltonian (16), its eigenvalues, and its eigenfunctions.

Consider Raman transitions between the QR states $|n = 0, \zeta = 1/2\rangle$ and $|n = 0, \zeta = -1/2\rangle$ that are split by an energy $\hbar\Delta_{\rm QR}$ by the presence of a rotation, or an external magnetic field, or an in-plane acceleration. When the red detuning $\Delta_{\rm hf}$ from the $F = 3/2$ hyperfine state is large enough, $|\Delta_{\rm hf}| \gg \gamma_{\rm hf}$ and $\Delta_{\rm hf} < 0$, where $\gamma_{\rm hf}$ is the decay rate of the $F = 3/2$ hyperfine state (see Fig. 4), the off-resonance intermediate $F = 3/2$ state can be eliminated and the Raman process can be treated as a two-level problem. The resultant generalized Raman Rabi frequency is given by $\Omega_g = \frac{\Omega_p\Omega_s}{\Delta_{\rm hf}}$. If we denote the energy difference between the two levels as $\hbar\Delta_{\rm QR}$, the detuning from Raman resonance is $\delta = \omega_p - \omega_s - \Delta_{\rm QR}$. The dressed-state two-level non-Hermitian Hamiltonian [21] which incorporates decay of the QR states can be written as [22]

$$H_{\rm Raman} = \mathcal{H}_{\rm Raman} - \frac{i\hbar}{2}\mathcal{G}, \tag{18}$$

where $\mathcal{H}_{\rm Raman}$ and $\mathcal{G}$ are 2×2 Hermitian matrices; the Hermitian part $\mathcal{H}_{\rm Raman}$ in (18) is

$$\mathcal{H}_{\rm Raman} = \hbar\begin{pmatrix} 0 & \Omega_g/2 \\ \Omega_g/2 & \delta \end{pmatrix}. \tag{19}$$

It acts in the two-dimensional Hilbert states spanned by $(1, 0)^T = |0, 1/2\rangle$ and $(0, 1)^T = |0, -1/2\rangle$. The anti-Hermitian part originates from the decay rate in the optical lattice:

$$\Gamma(\mathbf{r}) = \frac{\gamma_{\rm e}}{2\hbar\Delta}\{\tilde{V}(r) + F_r\tilde{B}(r)\}, \tag{20}$$

where $\gamma_{\rm e}$ is the decay rate of the excited $^2P_{3/2}$ state, and Δ is the detuning of the laser frequency from the resonant frequency. When $|\Delta| \gg \gamma_{\rm e}$, we can apply perturbation theory and write the anti-Hermitian part of the Hamiltonian (18) as

$$\mathcal{G}_{\zeta,\zeta'} = \int \Psi^\dagger_{0,\zeta}(\mathbf{r})\Gamma(\mathbf{r})\Psi_{0,\zeta'}(\mathbf{r})d^2\mathbf{r},$$

where $\Psi_{n,\zeta}(\mathbf{r})$ are the wave functions of the QR given by Eq. (10). Note that the atom in the quantum state with $\zeta = 1/2$ or $-1/2$ orbits clockwise or counterclockwise around the minimum of the lattice potential. The decay rate (20) is isotropic. Therefore, taking into account the symmetry of the wave function

$$\Psi_{n,-\zeta}(r, \phi) = F_x\Psi_{n,\zeta}(r, -\phi)$$

(which is true for $F = 1/2$ atoms), we can write

$$\mathcal{G}_{\zeta,\zeta'} = \Gamma_{0,1/2}\delta_{\zeta,\zeta'}, \tag{21}$$

where $\Gamma_{0,1/2}$ is given by Eq. (17). Equations (18), (19), and (21) yield Eq. (16).

Another source of uncertainty is spontaneous decay of the $F = 3/2$ hyperfine state, which gives a decay rate

$$\Gamma_{\rm hf} = \frac{\gamma_{\rm hf}}{\hbar\Delta_{\rm hf}}\sum_\sigma\int\left\{\tilde{V}(r) + \frac{{\rm sign}(\sigma)}{2}\tilde{B}(r)\right\} \times \psi^2_{0,1/2,\sigma}(r)dr. \tag{22}$$

For ^{6}Li atoms in the ground state, $\gamma_{\rm hf} = 1.586 \times 10^{-17}\,{\rm s}^{-1}$ [23]. Comparing Eqs. (17) and (22), one concludes that

$$\frac{\gamma_{\rm hf}}{\Delta_{\rm hf}} \ll \frac{\gamma_{\rm e}}{\Delta_{\rm e}},$$

hence $\Gamma_{\rm hf} \ll \Gamma_{0,1/2}$. Thus, in the following discussions we neglect $\Gamma_{\rm hf}$ since it is very small in comparison with $\Gamma_{0,1/2}$.

Eigenfunctions of the non-Hermitian Hamiltonian (16) are

$$|\psi_+\rangle = \mathcal{U}|0, 1/2\rangle + \mathcal{V}|0, -1/2\rangle, \tag{23a}$$

$$|\psi_-\rangle = \mathcal{V}|0, 1/2\rangle - \mathcal{U}|0, -1/2\rangle, \tag{23b}$$

where

$$\mathcal{U} = \sqrt{\frac{\tilde{\Omega} + \delta}{2\tilde{\Omega}}}, \quad \mathcal{V} = \sqrt{\frac{\tilde{\Omega} - \delta}{2\tilde{\Omega}}}, \quad \tilde{\Omega} = \sqrt{\delta^2 + \Omega_g^2}.$$

The corresponding eigenvalues are

$$\epsilon_\pm = \frac{\hbar(\delta - i\Gamma_{0,1/2})}{2} \pm \frac{\hbar\tilde{\Omega}}{2}.$$

The difference $\epsilon_+ - \epsilon_- = \hbar\tilde{\Omega}$ does not depend on $\Gamma_{0,1/2}$.

The time evolution of the wave function of the QR with time, starting with the initial wave function $|0, 1/2\rangle$, is specified by the time-dependent wave function

$$|\psi(t)\rangle = e^{-(\Gamma_{0,1/2}+i\delta)t/2} \times\left\{\left[\cos\left(\frac{\tilde{\Omega}t}{2}\right) + \frac{i\delta}{\tilde{\Omega}}\sin\left(\frac{\tilde{\Omega}t}{2}\right)\right]|0, 1/2\rangle - \frac{i\Omega_g}{\tilde{\Omega}}\sin\left(\frac{\tilde{\Omega}t}{2}\right)|0, -1/2\rangle\right\}. \tag{24}$$

The probabilities $P_{0,\pm1/2}(t)$ to find the QR in the states $|0, \pm1/2\rangle$ are given by $P_{0,\pm1/2}(t) = |\langle 0, \pm1/2|\psi(t)\rangle|^2$. Using Eq. (24), we find

$$P_{0,1/2}(t) = \left[1 - P_0\sin^2\left(\frac{\tilde{\Omega}t}{2}\right)\right]e^{-\Gamma_{0,1/2}t}, \tag{25a}$$

$$P_{0,-1/2}(t) = P_0\sin^2\left(\frac{\tilde{\Omega}t}{2}\right)e^{-\Gamma_{0,1/2}t}, \tag{25b}$$

where

$$P_0 = \frac{\Omega_g^2}{\tilde{\Omega}^2} = \frac{\Omega_g^2}{\delta^2 + \Omega_g^2}.$$

The Ramsey time-separated oscillating field method [24] with Raman pulses [25] using radio-frequency pump and Stokes radiation can be used to determine $\Delta_{\rm QR}$, as we shall now show.

The probability $P_{0,-1/2}(t)$ is plotted in Fig. 5 for different values of $|\delta|$. The amplitude P_0 of $P_{0,-1/2}(t)$ is maximal when $\delta = 0$. This is because P_0 is maximum when $\delta = 0$ ($\Delta_{\rm QR} = \omega_p - \omega_s$), and becomes very small for weak stimulated Raman scattering, i.e., when $|\delta| \gg \Omega_g$. Experimentally scanning ω_s and finding $\omega_p - \omega_s$ where $P_{0,-1/2}(t)$ is maximal yields $\Delta_{\rm QR}$.

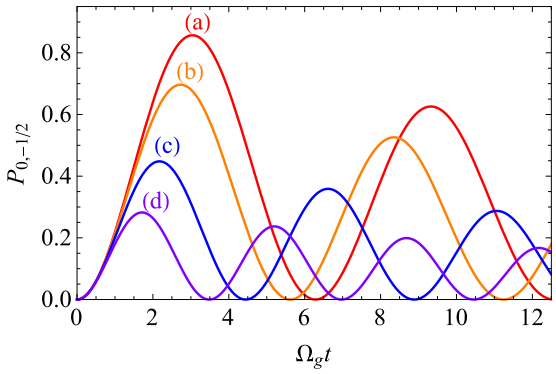

FIG. 5. The probability $P_{0,-1/2}(t)$ in Eq. (25b) to find the QR in the state $|0,-1/2\rangle$ as a function of time for $\Gamma_{0,1/2} = 0.05\,\Omega_g$, $\Omega_g = 1$, and different values of $|\delta|$: (a) $\delta = 0$, (b) $|\delta| = 0.5\,\Omega_g$, (c) $|\delta| = \Omega_g$, and (d) $|\delta| = 1.5\,\Omega_g$.

B. Ramsey separated oscillating field method

A preferable method of experimentally determining $\Delta_{\rm QR}$ is to employ the Ramsey time-separated oscillating field method [24] with Raman pulses [25]. The QR initially in the ground state $|0,1/2\rangle$ is subjected to two sets of Raman pulses of duration τ_p separated by a delay time T, so the generalized Rabi frequency becomes time dependent:

$$\Omega_g(t) = \begin{cases} \Omega_g & \text{if } 0 \leqslant t \leqslant \tau_p\,, \\ 0 & \text{if } \tau_p < t < T + \tau_p\,, \\ \Omega_g & \text{if } T + \tau_p \leqslant t \leqslant T + 2\tau_p\,, \end{cases} \tag{26}$$

with $\Omega_g \tau_p \approx \pi/2$ and $T \gg \tau_p$. The effect of the first pulse is to evolve the initial state into a coherent superposition of the initial and final states. During the delay time between pulses, the system carries out phase oscillations. Finally, the second pulse rotates the state vector again by an angle of $\Omega_g \tau_p$. Fixing the delay time T and measuring the population in the final state as a function of the detuning δ at the final time $T + 2\tau_p$ yields a fringe pattern as shown in Fig. 6. The figure shows the Ramsey fringes obtained for a single QR and the value of $\Delta_{\rm QR}$ such that $\delta = 0$ is easy to identify from the fringe pattern.

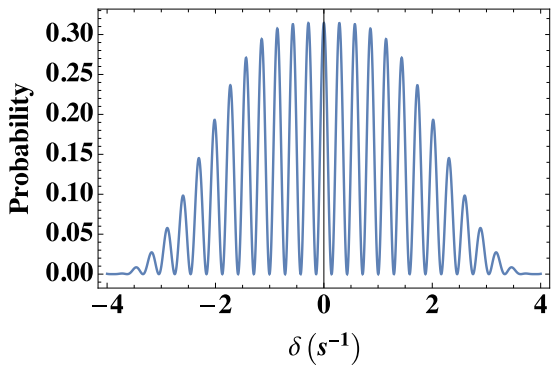

FIG. 6. Ramsey fringes in the probability $P_{|0,-1/2\rangle}$ at the final time $T + 2\tau_p$ plotted vs detuning δ. The splitting $\Delta_{\rm QR}$ is found by identifying where the detuning $\delta = \omega_p - \omega_s - \Delta_{\rm QR} = 0$.

IV. MAGNETOMETER

Atomic magnetometers often rely on a measurement of the Larmor precession of spin-polarized atoms in a magnetic field [26]. One of the limitations on their sensitivity is spin relaxation. In our system, spin relaxation is highly suppressed if the lattice is singly occupied.

The degenerate ground state of a fermionic QR is split by the external field, and measuring the frequency splitting can accurately determine the external field. When the QR is placed in an external magnetic field, say $B_{\rm ex}\mathbf{e}_z$ (for simplicity), a Zeeman interaction term, $H_B = -g\mu_B B_{\rm ex} F_z$, must be included in the Schrödinger equation (8). The energy of the ground state calculated to first order in $B_{\rm ex}$ is

$$\epsilon_{0,\zeta}(B_{\rm ex}) = \epsilon_{0,\zeta} + \frac{2\zeta g\mu_B B_{\rm ex}}{2I+1}\beta^z_{0,1/2}, \tag{27}$$

with $V_0 = 100\,\mathcal{E}_0$ and $B_0 = 180\,\mathcal{E}_0$, $\beta^z_{0,1/2} = 0.1078$. Equation (27) shows that the external magnetic field splits the degeneracy of the energy levels with $\zeta = \pm 1/2$. The Raman scattering between these levels gives rise to Rabi oscillations with amplitude that has a maximum when $\omega_p - \omega_s = \Delta_B$, where

$$\Delta_B = \frac{g\mu_B B_{\rm ex}}{(2I+1)\hbar}\beta^z_{0,1/2}. \tag{28}$$

The frequency splitting Δ_B can be experimentally measured, therefore the QR can be used as a magnetometer: measuring Δ_B and comparing with Eq. (28) yields the external magnetic field $B_{\rm ex}$. The uncertainty of $B_{\rm ex}$ results largely from the uncertainty of $\beta^{(z)}_{0,1/2}$ which is a function of the laser frequency ω and amplitude E_0. Hence, the accuracy of measuring $B_{\rm ex}$ is

$$\frac{\delta B_{\rm ex}}{B_{\rm ex}} = \frac{1}{\beta^z_{0,1/2}}\sqrt{\left(\frac{\partial\beta^z_{0,1/2}}{\partial\omega}\delta\omega\right)^2 + \left(\frac{\partial\beta^z_{0,1/2}}{\partial E_0}\delta E\right)^2}, \tag{29}$$

where $\delta\omega$ and δE are the uncertainties of ω and E_0. Additional analysis of $\delta B_{\rm ex}$, including the suppression of spin relaxation in a singly occupied optical lattice [27,28], directional external magnetic field effects, the lack of spectral line splitting due to the small anisotropy of the effective lattice potential, and measurement-time limitations, is provided in Sec. VII.

V. ROTATION SENSOR

When the QR is in a noninertial frame rotating with an angular velocity $\boldsymbol{\Omega}$ there is an additional term $H_\Omega = \hbar\boldsymbol{\Omega}\cdot\boldsymbol{\mathcal{L}}$ in the Hamiltonian, where $\boldsymbol{\mathcal{L}} = \mathbf{F} + \boldsymbol{\ell}$. For $\boldsymbol{\Omega}$ along the z axis, the QR energy is

$$\epsilon_{0,\zeta}(\Omega_z) = \epsilon_{0,\zeta} + \zeta\hbar\Omega_z. \tag{30}$$

In fact, for arbitrary $\boldsymbol{\Omega}$, Eq. (30) is valid to first order in $\boldsymbol{\Omega}$ (see Appendix E for details). The splitting of the ground-state energy is $\Delta_\Omega = \Omega_z$, and the accuracy of measurement of the angular velocity due to spontaneous magnetic dipole transitions within the ground-state QR manifold is $\delta\Omega_z = \delta\Delta_\Omega = 4g^2\mu_B^2\Omega_z^3/(3\hbar c^3)$. Additional analysis of $\delta\Omega_z$, including the suppression of spin relaxation in a singly occupied optical lattice [27,28], the lack of spectral line splitting due

to the small anisotropy of the effective lattice potential, and measurement-time limitations, is given in Sec. VII.

VI. ACCELEROMETER

When the QR is in a noninertial frame moving with a linear acceleration **a**, an additional term $H_a = M\mathbf{a}\cdot\mathbf{r}$ must be included in the Hamiltonian. The energy of the ground state calculated to first order in **a** is

$$\epsilon_{0,\zeta}(a_\parallel) = \epsilon_{0,\zeta} + \zeta M a_\parallel \varrho_{0,\zeta}, \tag{31}$$

where $\varrho_{n,\zeta} = \int[\psi^2_{n,\zeta,1/2}(r) + \psi^2_{n,\zeta,-1/2}(r)]rdr$. The splitting of the ground-state energy is $\Delta_a = Ma_\parallel\varrho_{0,\zeta}/\hbar$. The acceleration measurement accuracy $\delta a_\parallel$ is considered in Sec. VII.

VII. ACCURACY ESTIMATES FOR B_{ex}, Ω, AND a

A. Magnetometer

The uncertainty of B_{ex} results largely from the uncertainty of the quantity $\beta^z_{0,1/2}$ which is a function of the laser frequency ω and amplitude E_0. Hence, the accuracy of measuring B_{ex} is given by Eq. (29). It is convenient to rewrite Eq. (29) as

$$\frac{\delta B_{ex}}{B_{ex}} = \frac{1}{\beta^z_{0,1/2}}\sqrt{\left(\frac{\partial\beta^z_{0,1/2}}{\partial\mathcal{E}_0}\delta\mathcal{E}\right)^2 + \left(\frac{\partial\beta^z_{0,1/2}}{\partial\mathcal{I}_0}\delta\mathcal{I}\right)^2}, \tag{32}$$

where $\delta\mathcal{E}$ and $\delta\mathcal{I}$ are uncertainties of the recoil energy $\mathcal{E}_0$ and the laser intensity $\mathcal{I}_0$. $\beta^z_{0,1/2}$ depends on a single parameter, $\mathcal{I}_0/\mathcal{E}_0$, therefore

$$\mathcal{E}_0\frac{\partial\beta^z_{0,1/2}}{\partial\mathcal{E}_0} = -\mathcal{I}_0\frac{\partial\beta^z_{0,1/2}}{\partial\mathcal{I}_0}.$$

Assuming that $\delta\mathcal{I}/\mathcal{I}_0 \ll \delta\omega/\omega$, we get

$$\frac{\delta B_{ex}}{B_{ex}} = \frac{\delta\mathcal{E}}{\beta^z_{0,1/2}}\left|\frac{\partial\beta^z_{0,1/2}}{\partial\mathcal{E}_0}\right|.$$

Numerical calculations for $V_0 = 100\,\mathcal{E}_0$ and $B_0 = 180\,\mathcal{E}_0$ give

$$\frac{\delta B_{ex}}{B_{ex}} = -\frac{0.075495\delta\omega}{\omega},$$

where we have used the fact that $\delta\mathcal{E}/\mathcal{E}_0 = 2\,\delta\omega/\omega$. For lithium atoms, $\omega = 2.808\times10^{15}$ s^{-1} [29], and taking $\delta\omega = 2\pi\times 160$ mHz $= 1.005$ s^{-1} [30] we find

$$\frac{\delta B_{ex}}{B_{ex}} = 2.703\times10^{-17}. \tag{33}$$

B. Rotation sensor

As already stated in Sec. V, the accuracy of measurement of the angular velocity due to spontaneous magnetic dipole transitions within the ground-state QR manifold is $\delta\Omega_z = 4g^2\mu_B^2\Omega_z^3/(3\hbar c^3)$, hence

$$\frac{\delta\Omega_z}{\Omega_z^3} = 1.614\times10^{-44}\,\mathrm{s}^2. \tag{34}$$

For $\Omega_z = 72.722$ μrad/s (the rotation frequency of Earth), $\delta\Omega_z = 6.209\times10^{-57}$ s^{-1}.

C. Accelerometer

The acceleration measurement accuracy $\delta a_\parallel$ is given by

$$\frac{\delta a_\parallel}{a_\parallel} = \frac{1}{\varrho_{0,1/2}}\sqrt{\left(\frac{\partial\varrho_{0,1/2}}{\partial\omega}\delta\omega\right)^2 + \left(\frac{\partial\varrho_{0,1/2}}{\partial E_0}\delta E\right)^2}. \tag{35}$$

Taking into account the equalities,

$$\frac{\partial\varrho_{0,1/2}}{\partial\omega}\delta\omega = \frac{\partial\varrho_{0,1/2}}{\partial\mathcal{E}_0}\delta\mathcal{E},$$
$$\frac{\partial\varrho_{0,1/2}}{\partial E_0}\delta E = \frac{\partial\varrho_{0,1/2}}{\partial\mathcal{I}_0}\delta\mathcal{I},$$

where $\mathcal{E}_0$ is the recoil energy (D3) and $\mathcal{I}_0 \propto E_0^2$ is the intensity of the laser beam. Assuming that

$$\left|\frac{\partial\varrho_{0,1/2}}{\partial\mathcal{I}_0}\right|\delta\mathcal{I} \ll \left|\frac{\partial\varrho_{0,1/2}}{\partial\mathcal{E}_0}\right|\delta\mathcal{E},$$

we find that

$$\frac{\delta a_\parallel}{a_\parallel} \approx \frac{\delta\mathcal{E}}{\varrho_{0,1/2}}\left|\frac{\partial\varrho_{0,1/2}}{\partial\mathcal{E}_0}\right|.$$

Numerical calculations for $V_0 = 100\,\mathcal{E}_0$ and $B_0 = 180\,\mathcal{E}_0$ give

$$\frac{1}{\varrho_{0,1/2}}\left|\frac{\partial\varrho_{0,1/2}}{\partial\mathcal{E}_0}\right| = \frac{0.139986}{\mathcal{E}_0},$$

hence

$$\frac{\delta a_\parallel}{a_\parallel} = 1.002\times10^{-16}.$$

The measurement accuracies of an external magnetic field, angular velocity, and linear acceleration are also affected by the energy-time uncertainty principle. Given a measurement time T, the measurement bandwidth is $1/(2T)$, and the accuracy of the QR magnetometer, accelerometer, or gyroscope is proportional to $1/\sqrt{T}$ [31]. For an optical lattice with N QRs, the accuracies of the magnetometer, gyroscope, and accelerometer are [31]

$$\delta B_u = \frac{B_{ex}}{\beta^z_{0,1/2}}\left|\frac{\partial\beta^z_{0,1/2}}{\partial\omega}\right|\sqrt{\frac{\delta\omega}{NT}}, \tag{36}$$

$$\delta\Omega_u = \sqrt{\frac{\delta\Omega_z}{NT}}, \tag{37}$$

$$\delta a_u = \frac{a_\parallel}{\varrho_{0,1/2}}\left|\frac{\partial\varrho_{0,1/2}}{\partial\omega}\right|\sqrt{\frac{\delta\omega}{NT}}. \tag{38}$$

Here the subscript u denotes uncertainty due to the finite measurement time, $\delta\omega$ is the uncertainty of the optical lattice laser frequency ω, and $\delta\Omega_z$ is the angular velocity uncertainty given by Eq. (34). Taking $T = 1$ s, and $N = 4.99\times10^8$ (which corresponds to an optical lattice of area 1 cm^2), we get

$$\frac{\delta B_u}{B_{ex}} = 1.74\times10^{-20}, \tag{39}$$

$$\frac{\delta\Omega_u}{\Omega_z^{3/2}} = 5.687\times10^{-27}\,\mathrm{s}^{1/2}, \tag{40}$$

$$\frac{\delta a_u}{a_\parallel} = 4.474\times10^{-21}. \tag{41}$$

VIII. UNCERTAINTY DUE TO SHOT NOISE IN THE STOKES AND PUMP PULSES

Another source of uncertainty $\delta B_{\rm ex}$, $\delta\Omega$, and δa arises from shot noise in the Stokes and pump pulses used to measure the detuning $\Delta_{\rm QR}$ of the QR using the Ramsey separated field method (see Figs. 4 and 6). Shot noise results in fluctuations in the position and amplitude of the population oscillations of the Ramsey fringes because the $\pi/2$ Raman pulses have Rabi frequencies which fluctuate, $\Omega_R\tau$:

$$\phi_R \equiv \Omega_R\tau = \frac{\pi}{2} \pm \delta\phi_R,$$

where

$$\delta\phi_R \lesssim \frac{\pi}{2}\left(\frac{1}{\sqrt{N_p}} + \frac{1}{\sqrt{N_s}}\right), \tag{42}$$

and N_p and N_s are the number of photons of the pump and Stokes beams, assuming a Poissonian distribution of photon number. The uncertainty $\delta\Delta_{\rm QR}$ of $\Delta_{\rm QR}$ can be estimated from the variation of the probability for population transfer from the initial level of the split QR ground-state level to the final level. A simple calculation shows that

$$\delta\Delta_{\rm QR} \lesssim \frac{\sqrt{1.5}\,\delta\phi_R}{\tau} \lesssim \frac{1.92}{\tau}\left(\frac{1}{\sqrt{N_p}} + \frac{1}{\sqrt{N_s}}\right), \tag{43}$$

where we have used (42) for $\delta\phi_R$.

The ground-state hyperfine splitting of lithium atoms is $\omega_{\rm hf} = 2\pi \times 228.2$ MHz $= 1.434 \times 10^9$ s^{-1}, so the energies of Stokes and pump photons are $\hbar\omega_s \lesssim \hbar\omega_p \lesssim \hbar\omega_{\rm hf}$, where $\hbar\omega_{\rm hf} = 1.51226 \times 10^{-18}$ erg. The numbers of photons N_p and N_s can be estimated as

$$N_\nu = \frac{\pi r_b^2 \tau I_\nu}{\hbar\omega_\nu}, \tag{44}$$

where I_ν is the intensity of the pump ($\nu = p$) or Stokes ($\nu = s$) field, r_b is the radius of the beam (which is assumed to be the same for the pump and Stokes beams), and τ is the pulse duration. Taking $I_p = 5 \times 10^3$ W/m^2, $I_s = 2 \times 10^4$ W/m^2, we get $\tau = 1.644$ ms. For $r_b \approx 0.2$ m (the microwave wavelength), the numbers of photons (44) are

$$N_p \approx 7.467 \times 10^{24}, \qquad N_s \approx 2.987 \times 10^{25},$$

so from Eq. (43) $\delta\Delta_{\rm QR}$ is

$$\delta\Delta_{\rm QR} \approx 6.411 \times 10^{-10}\ {\rm s}^{-1} = 2\pi \times 0.102\ {\rm nHz}.$$

Knowing $\Delta_{\rm QR}$, the external magnetic field $B_{\rm ex}$, the angular velocity Ω, or the acceleration a of the noninertial frame can be calculated using

$$B_{\rm ex} = \frac{(2I+1)\hbar\Delta_{\rm QR}}{g\mu_B\beta^z_{0,1/2}}, \tag{45}$$

$$\Omega = \Delta_{\rm QR}, \tag{46}$$

$$a = \frac{\hbar\Delta_{\rm QR}}{M\varrho_{0,1/2}}. \tag{47}$$

Here $I = 1$ is the nuclear spin of ^{6}Li atoms, $\beta^z_{0,1/2} = 0.1078$, M is the atomic mass, and $\varrho_{0,1/2} = 0.0987\lambda_0$, where λ_0 is the wavelength of the laser beam creating the optical lattice. For ^{6}Li atoms, $\lambda_0 = 670.964$ nm, and therefore $\varrho_{0,1/2} = 66.18$ nm.

When the optical lattice has N quantum rotors, uncertainties of external magnetic field $B_{\rm ex}$, angular velocity Ω, and acceleration a due to the shot noise are given by

$$\delta B_{\rm ex} = \frac{1}{\sqrt{N}}\frac{(2I+1)\hbar\,\delta\Delta_{\rm QR}}{g\mu_B\beta^z_{0,1/2}}, \tag{48}$$

$$\delta\Omega = \frac{\delta\Delta_{\rm QR}}{\sqrt{N}}, \tag{49}$$

$$\delta a = \frac{1}{\sqrt{N}}\frac{\hbar\,\delta\Delta_{\rm QR}}{M\varrho_{0,1/2}}. \tag{50}$$

For $N = 4.99 \times 10^8$ ^{6}Li atoms,

$$\delta B_{\rm ex} = 4.54 \times 10^{-24}\ {\rm T},$$
$$\delta\Omega = 2.87 \times 10^{-14}\ {\rm s}^{-1},$$
$$\delta a = 4.58 \times 10^{-15}\ {\rm m/s}^2.$$

Compare this result with the uncertainties of the magnetic field and angular velocity of the Earth, and the acceleration due to gravity derived in Sec. VII:

$$\delta B_u = 7.8 \times 10^{-25}\ {\rm T},$$
$$\delta\Omega_u = 3.6 \times 10^{-33}\ {\rm s}^{-1},$$
$$\delta a_u = 4.4 \times 10^{-20}\ {\rm m/s}^2.$$

Hence the shot-noise contribution to the uncertainty is larger than the uncertainty due to the decay rate of the excited hyperfine state.

IX. SUMMARY AND CONCLUSIONS

The wave functions of QRs, atoms trapped by a SDOLP, are confined to circular rings of radius r_0 with center at the minima of the scalar lattice potential. SDOLPs with precisely one atom per site (which suppress spin relaxation) can be used as ultrahigh accuracy rotation sensors, accelerometers, or magnetometers. The Ramsey time-separated oscillating field method with far-off-resonance Raman pulses between the split ground state of fermionic QRs can be used as a spectroscopic measurement technique for these applications, with a major accuracy limitation due to measurement-time uncertainty as outlined in Secs. VII and VIII. Bosonic QRs have ground states which are not degenerate, but their excited states are degenerate. The splitting of the excited states in the presence of rotation, in-plane acceleration, or magnetic fields can also be used for sensing.

ACKNOWLEDGMENT

This work was supported in part by a grant from the Deutsche Forschungsgemeinschaft through the DIP program (Grant No. FO703/2-1).

APPENDIX A: OPTICAL LATTICE POTENTIAL

Consider a 2D hexagonal optical lattice potential produced by six coherent laser beams having a superposition of in-plane and out-of-plane linear polarization with a configuration

shown in Fig. 1. Note that other configurations, e.g., three or four laser beams instead of six, can also produce a SDOLP, but we shall not consider other configurations here. The wavelength, wave number, and frequency of the laser beams are λ_0, $q_0 = 2\pi/\lambda_0$, and $\omega_0 = q_0 c$, where c is the speed of light. The optical lattice frequency should be slightly detuned to the red of resonance. For ^{6}Li atoms, the resonant wavelength is $\lambda_{\rm res} = 670.963$ nm. The resultant electric field is given by $\mathbf{E}(\mathbf{r}, t) = [\mathbf{E}(\mathbf{r})e^{-i\omega_0 t} + \text{c.c.}]/2$ where the spatial dependence of the field is

$$\mathbf{E}(\mathbf{r}) = E_0 \sum_{n=1}^{6} \boldsymbol{\xi}_n e^{i\mathbf{q}_n \mathbf{r}}. \tag{A1}$$

The wave vectors $\mathbf{q}_n$ are

$$\begin{aligned} \mathbf{q}_1 &= -\mathbf{q}_4 = -q_0\,\mathbf{e}_x, \\ \mathbf{q}_2 &= -\mathbf{q}_5 = -\frac{q_0}{2}\{\mathbf{e}_x + \sqrt{3}\,\mathbf{e}_y\}, \\ \mathbf{q}_3 &= -\mathbf{q}_6 = \frac{q_0}{2}\{\mathbf{e}_x - \sqrt{3}\,\mathbf{e}_y\}, \end{aligned} \tag{A2}$$

and the unit vectors $\mathbf{e}_x$, $\mathbf{e}_y$, and $\mathbf{e}_z$ are parallel to the x, y, and z axes. The polarization vectors $\boldsymbol{\xi}_n$ $(1 \leqslant n \leqslant 6)$ are $\boldsymbol{\xi}_n = \{\sqrt{1-\beta^2}\mathbf{e}_z + \frac{\beta}{q_0}[\mathbf{q}_n \times \mathbf{e}_z]\}$, where β is real and lies in the interval $0 < \beta \leqslant 1/\sqrt{2}$. Hereafter, we take $\beta = 1/\sqrt{2}$.

For an arbitrary atom with electronic angular momentum $\mathbf{J}$, the electric field generates an effective SDOLP [9]:

$$\begin{aligned} U(\mathbf{r}) = -\frac{1}{4}\Bigg(&\alpha^s_{n,J}(\omega_0)\,\mathbf{E}^*(\mathbf{r})\cdot\mathbf{E}(\mathbf{r}) \\ &- \frac{i\alpha^v_{n,J}(\omega_0)}{2J}\,[\mathbf{E}^*(\mathbf{r})\times\mathbf{E}(\mathbf{r})]\cdot\mathbf{J} \\ &+ \frac{3\alpha^t_{n,J}(\omega_0)}{2J(2J-1)}\Big\{[\mathbf{E}^*(\mathbf{r})\cdot\mathbf{J}]\,[\mathbf{E}(\mathbf{r})\cdot\mathbf{J}] \\ &+ [\mathbf{E}(\mathbf{r})\cdot\mathbf{J}]\,[\mathbf{E}^*(\mathbf{r})\cdot\mathbf{J}] \\ &- \frac{2}{3}J(J+1)\,\mathbf{E}^*(\mathbf{r})\cdot\mathbf{E}(\mathbf{r})\Big\}\Bigg), \end{aligned} \tag{A3}$$

where U is a $(2J+1)\times(2J+1)$ matrix in spin space. Here $\alpha^s_{n,J}(\omega_0)$, $\alpha^v_{n,J}(\omega_0)$, and $\alpha^t_{n,J}(\omega_0)$ are the conventional dynamical scalar, vector, and tensor polarizabilities of the atom in the fine-structure level $|nJ\rangle$ with principal quantum number n and total electronic angular momentum J [9]:

$$\alpha^s_{n,J}(\omega_0) = \frac{\alpha^{(0)}_{n,J}(\omega_0)}{\sqrt{3(2J+1)}}, \tag{A4}$$

$$\alpha^v_{n,J}(\omega_0) = -\frac{\sqrt{2J}\,\alpha^{(1)}_{n,J}(\omega_0)}{\sqrt{(J+1)(2J+1)}}, \tag{A5}$$

$$\alpha^t_{n,J}(\omega_0) = -\frac{\sqrt{2J(2J-1)}\,\alpha^{(2)}_{n,J}(\omega_0)}{\sqrt{3(J+1)(2J+1)(2J+3)}}. \tag{A6}$$

The terms on the right-hand side of Eq. (A3) proportional to $\alpha^s_J(\omega_0)$, $\alpha^v_J(\omega_0)$, and $\alpha^t_J(\omega_0)$ describe a spin-independent optical lattice potential, a Zeeman-type interaction, and a tensor Stark-type interaction, respectively. The scalar $\alpha^{(0)}_{n,J}(\omega_0)$, vector $\alpha^{(1)}_{n,J}(\omega_0)$, and tensor $\alpha^{(2)}_{n,J}(\omega_0)$ polarizabilities of the atom in the fine-structure level $|nJ\rangle$ can be calculated as follows [9]:

$$\begin{aligned} \alpha^{(K)}_{n,J}(\omega_0) = (-1)^{K+J+1}\sqrt{2K+1}\sum_{n',J'}(-1)^{J'} \\ \times \begin{Bmatrix} 1 & K & 1 \\ J & J' & J \end{Bmatrix} |\langle n'J'\|\mathbf{d}\|nJ\rangle|^2 \\ \times \frac{1}{\hbar}\,\mathrm{Re}\Bigg(\frac{1}{\omega_{n',J';n,J} - \omega_0 - i\gamma_{n',J';n,J}/2} \\ + \frac{(-1)^K}{\omega_{n',J';n,J} + \omega_0 + i\gamma_{n',J';n,J}/2}\Bigg). \end{aligned} \tag{A7}$$

Here $K = 0, 1, 2$ gives the scalar, vector, and tensor polarizabilities, $\{\begin{smallmatrix} 1 & K & 1 \\ J & J' & J \end{smallmatrix}\}$ is the Wigner 6-j symbol, and $\langle nJ \parallel \mathbf{d} \parallel n'J'\rangle$ denotes the reduced matrix elements of the dipole moment operator. The quantities $\omega_{n',J';n,J} = (\epsilon_{n',J'} - \epsilon_{n,J})/\hbar$ and $\gamma_{n',J';n,J} = \gamma_{n',J'} + \gamma_{n,J}$ are the angular frequency and linewidth of the transition between the fine-structure levels $|nJ\rangle$ and $|n'J'\rangle$.

1. Li atom scalar and vector polarizabilities

Equation (A7) contains an expression for the scalar and vector polarizabilities of an atom in terms of matrix elements of the dipole operator between electronic wave functions. Here we use this expression in the special case of $J = 1/2$ and compute the scalar and vector polarizabilities $\alpha_s(\omega)$ and $\alpha_v(\omega)$ of the Li atom in its ground state, the electronic configuration of which (outside the closed $1s$ shell) is $2s\,^2S_{1/2}$ [17]:

$$\alpha_0(\omega) = -\frac{\alpha^{(0)}_{2,1/2}(\omega)}{\sqrt{6}}, \tag{A8a}$$

$$\alpha_1(\omega) = \frac{\alpha^{(1)}_{2,1/2}(\omega)}{\sqrt{3}}, \tag{A8b}$$

where $\alpha^{(K)}_{n,J}(\omega)$ $(K = 0, 1)$ are the coupled polarizabilities given in Eq. (A7), whereas the tensor polarizability $\alpha^{(K=2)}_{n,J}(\omega) = 0$ (see Ref. [17] for details). For the calculations of the reduced matrix elements $\langle n'J'||\mathbf{d}||nJ\rangle$ we need the electronic wave function of the Li atom in its ground and excited states. The ground-state wave function with configuration $2s\,^2S_{1/2}$ is

$$\Psi_{S,m_s}(r) = \frac{1}{\sqrt{4\pi}}\,\psi_{2s}(r)\chi_{m_s}, \tag{A9}$$

where $\psi_{2s}(r)$ is the real valued radial wave function of the $2s$ electron and χ_{m_s} are spin-wave functions, $m_s = \pm 1/2$. The radial and spin-wave functions are normalized by the conditions $\int_0^\infty \psi^2_{2s}(r)r^2dr = 1$ and $\chi^\dagger_{m_s}\chi_{m'_s} = \delta_{m_s,m'_s}$.

The electronic wave functions of Li in the excited $2p\,^2P_{1/2}$ and $2p\,^2P_{3/2}$ states are given by

$$\begin{aligned} \Psi_{2p,J,m_J}(\mathbf{r}) = \psi_{2p}(r)\sum_{m_L,m_s} C^{J,m_J}_{1,m_L;1/2,m_s} \\ \times Y_{1,m_L}(\theta,\phi)\chi_{m_s}. \end{aligned} \tag{A10}$$

Here $\psi_{2p}(r)$ is the radial wave function of the $2p$ electron; $Y_{1,m_L}(\theta,\phi)$ are spherical harmonics with $m_L = 0, \pm 1$; χ_{m_s} are

TABLE II. The 6-j symbols for Li atoms in thew ground $^2S_{1/2}$ and excited $^2P_{3/2}$ states.

	J = 1/2	J = 3/2
$K=0$	$1/\sqrt{6}$	$-1/\sqrt{6}$
$K=1$	$-1/3$	$-1/6$

spin-wave functions with $m_s = \pm 1/2$; and

$$C^{J,m_J}_{1,m_L;1/2,m_s} \equiv \left\langle 1 m_L \tfrac{1}{2} m_s \middle| J m_J \right\rangle$$

are Clebsch-Gordan coefficients. The radial wave functions and the spherical harmonics are normalized by the conditions $\int_0^\infty \psi^2_{2p}(r) r^2 dr = 1$ and

$$\int_0^{2\pi} d\phi \int_0^{\pi} \sin\theta d\theta Y^*_{1,m_L}(\theta,\phi) Y_{1,m'_L}(\theta,\phi) = \delta_{m_L,m'_L}.$$

The reduced matrix element of the electric dipole moment operator is

$$d_0 \equiv |\langle eJ \| \mathbf{d} \| g 1/2 \rangle| = e \int_0^\infty \psi_{2s}(r)\psi_{2p}(r) r^3 dr. \quad \text{(A11)}$$

The 6-j symbols required in Eq. (A7) for the Li atom are $\{\begin{smallmatrix} 1 & K & 1 \\ 1/2 & J & 1/2 \end{smallmatrix}\}$ and are given by Table II.

We also need the resonant frequencies,

$$\omega_{J,1/2} = \frac{1}{\hbar}\{\epsilon_{\mathrm{p},J} - \epsilon_{\mathrm{s},1/2}\}, \quad J = \frac{1}{2}, \frac{3}{2},$$

where $\epsilon_{\mathrm{s},1/2}$ is the energy of the ground $^2S_{1/2}$ state, and $\epsilon_{\mathrm{p},J}$ are the energies of the excited ^2P_J states. The optical lattice frequency detuning from resonance should be smaller than the fine-structure splitting (to have a significant effective magnetic field) but larger than the linewidth of the transitions. Hence, we assume that the frequency ω satisfies the inequalities

$$\frac{\gamma_{J,1/2}}{2} \ll \omega_{3/2,1/2} - \omega \ll \omega_{3/2,1/2} - \omega_{1/2,1/2},$$

which imply

$$\frac{1}{\omega_{3/2,1/2} - \omega} \gg \frac{1}{\omega - \omega_{1/2,1/2}} \gg \frac{1}{\omega_{J,1/2} + \omega}.$$

The last inequality shows that the main contribution to the coupled polarizabilities (A7) is from $(\omega_{J,1/2} - \omega)^{-1}$ (where $J = 1/2, 3/2$), whereas the terms $(\omega_{J,1/2} + \omega)^{-1}$ can be neglected. As a result, the coupled polarizabilities (A7) are given by

$$\alpha^{(0)}_{2,1/2}(\omega) = -\frac{d_0^2}{\sqrt{6}\hbar}\frac{1}{\omega_{1/2,1/2} - \omega} - \frac{d_0^2}{\sqrt{6}\hbar}\frac{1}{\omega_{3/2,1/2} - \omega},$$

$$\alpha^{(1)}_{2,1/2}(\omega) = \frac{d_0^2}{\sqrt{3}\hbar}\frac{1}{\omega_{1/2,1/2} - \omega} - \frac{d_0^2}{2\sqrt{3}\hbar}\frac{1}{\omega_{3/2,1/2} - \omega}.$$

The scalar and vector polarizabilities (A8) are

$$\alpha_0(\omega) = \frac{d_0^2}{6\hbar}\frac{1}{\omega_{1/2,1/2} - \omega} + \frac{d_0^2}{6\hbar}\frac{1}{\omega_{3/2,1/2} - \omega}, \quad \text{(A12a)}$$

$$\alpha_1(\omega) = \frac{d_0^2}{3\hbar}\frac{1}{\omega_{1/2,1/2} - \omega} - \frac{d_0^2}{6\hbar}\frac{1}{\omega_{3/2,1/2} - \omega}. \quad \text{(A12b)}$$

The ratio of the vector and scalar polarizabilities is

$$\frac{\alpha_1(\omega)}{\alpha_0(\omega)} = \frac{2\omega_{3/2,1/2} - \omega_{1/2,1/2} - \omega}{\omega_{3/2,1/2} + \omega_{1/2,1/2} - 2\omega} \approx 2. \quad \text{(A13)}$$

2. Spin-dependent optical potential for $J = 1/2$

The effective SDOLP $U(\mathbf{r})$ in Eq. (A3) acts in the Hilbert space of atomic states spanned by the basis kets $|nJFf\rangle$ where the quantum number F corresponds to the total atomic angular momentum operator $\mathbf{F} = \mathbf{J} + \mathbf{I}$ and f is its projection on the z axis [9]. Generically, $U(\mathbf{r})$ is not diagonal in F or in f. However, when the off-diagonal elements with $F \neq F'$ are much smaller than the hyperfine energy splitting of the atoms, we can neglect them. Within the subspace of fixed n, J, F the matrix elements of $U(\mathbf{r})$ are written as

$$W_{f,f'}(\mathbf{r}) = \langle nJFf|U(\mathbf{r})|nJFf'\rangle.$$

As already stated, in the special case $J = 1/2$, $\alpha^{(K=2)}_{n,J}(\omega_0) = 0$, i.e., the tensor Stark-type interaction operator vanishes. Hence, the optical lattice potential $W_{f,f'}(\mathbf{r})$ takes the form [9]

$$W_{f,f'}(\mathbf{r}) = V(\mathbf{r})\delta_{f,f'} - \mathbf{B}(\mathbf{r}) \cdot \mathbf{F}_{f,f'}, \quad \text{(A14)}$$

where the scalar optical potential $V(\mathbf{r})$ and a *fictitious magnetic field* $\mathbf{B}(\mathbf{r})$ (which is taken to have units of energy) are given by Eq. (4). The scalar and vector dynamical polarizabilities of the atom are [9]

$$\alpha_0(\omega_0) = \frac{\alpha^{(0)}_{n,1/2}(\omega_0)}{\sqrt{6}}, \quad \text{(A15)}$$

$$\alpha_1(\omega_0) = (-1)^{I+1/2+F}\frac{\alpha^{(1)}_{n,1/2}(\omega_0)}{\sqrt{3}}. \quad \text{(A16)}$$

Substituting Eq. (A1) into Eq. (4a), and using polar coordinates $\mathbf{r} = (r,\phi)$, $x = r\cos\phi$, $y = r\sin\phi$, we obtain

$$V(\mathbf{r}) = -\frac{V_0}{3} - \frac{V_0}{6}\sum_{m=0}^{2}\cos\left[\frac{2\pi r}{\lambda_0}\cos(\phi - m\theta_0)\right] - \frac{V_0}{18}\sum_{m=0}^{2}\cos\left[\frac{2\sqrt{3}\pi r}{\lambda_0}\sin(\phi - m\theta_0)\right], \quad \text{(A17)}$$

where $\theta_0 = 2\pi/3$. The potential strength V_0 is given by

$$V_0 = \frac{9\alpha_0(\omega_0)}{2}E_0^2. \quad \text{(A18)}$$

Substituting Eq. (A1) into Eq. (4b), we get

$$\mathbf{B}(\mathbf{r}) = B_r(\mathbf{r})\mathbf{e}_r + B_\phi(\mathbf{r})\mathbf{e}_\phi. \quad \text{(A19)}$$

The components $B_r(\mathbf{r})$ and $B_\phi(\mathbf{r})$ of $\mathbf{B}(\mathbf{r})$ are expanded as

$$B_r(\mathbf{r}) = \frac{B_0}{9(2I+1)}\sum_{m=0}^{3}\cos(\phi + m\theta_0) \times \sin\left[\frac{2\pi r}{\lambda_0}\cos(\phi - m\theta_0)\right] + \frac{B_0}{3\sqrt{3}(2I+1)}\sum_{m=0}^{2}\sin(\phi - m\theta_0)$$

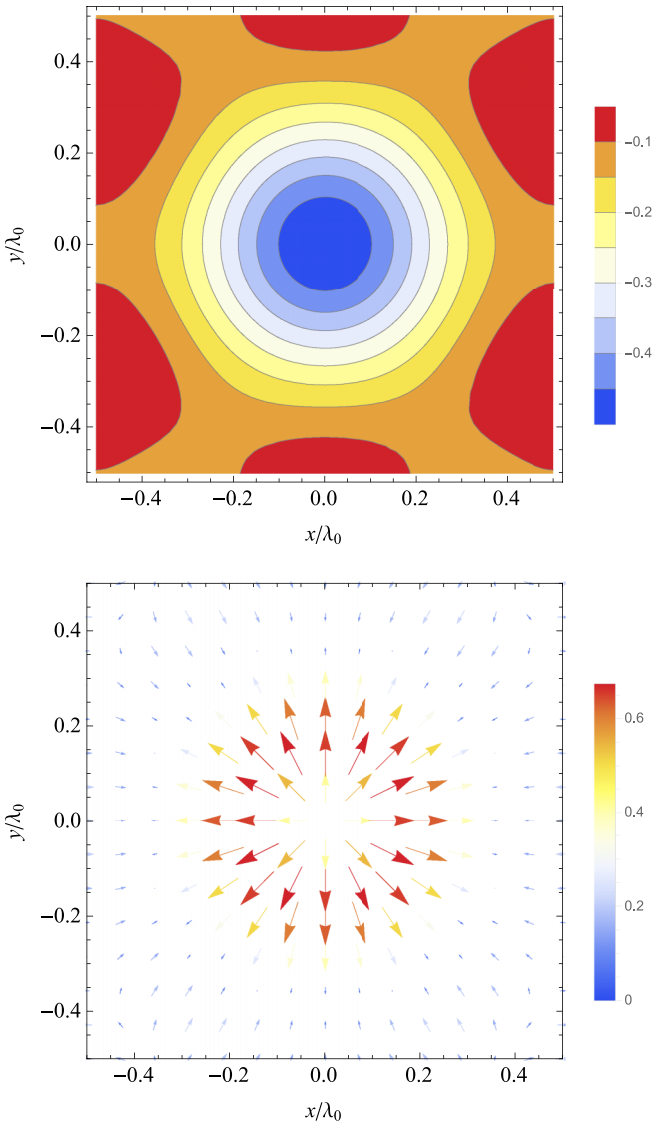

FIG. 7. (a) The optical lattice potential $V(\mathbf{r})$, Eq. (A17), and (b) the fictitious magnetic field (A19) as functions of the Cartesian coordinates x and y for $\beta = 1/\sqrt{2}$. The plot legends denote (a) $V(\mathbf{r})/V_0$ (contour plot with minimum indicated by deep blue). (b) $|\mathbf{B}(\mathbf{r})|/B_0$ (direction and strength indicated by arrows of varying length and color). V_0 and B_0 are given by Eqs. (A18) and (A21).

$$\times \sin\left[\frac{2\sqrt{3}\pi r}{\lambda_0}\sin(\phi - m\theta_0)\right] + \frac{B_0}{9(2I+1)}\sum_{m=0}^{2}\cos(\phi - m\theta_0) \times \sin\left[\frac{4\pi r}{\lambda_0}\cos(\phi - m\theta_0)\right], \tag{A20a}$$

$$B_\phi(\mathbf{r}) = -\frac{B_0}{9(2I+1)}\sum_{m=0}^{3}\sin(\phi + m\theta_0) \times \sin\left[\frac{2\pi r}{\lambda_0}\cos(\phi - m\theta_0)\right] + \frac{B_0}{3\sqrt{3}(2I+1)}\sum_{m=0}^{2}\cos(\phi - m\theta_0) \times \sin\left[\frac{2\sqrt{3}\pi r}{\lambda_0}\sin(\phi - m\theta_0)\right] + \frac{B_0}{9(2I+1)}\sum_{m=0}^{2}\sin(\phi - m\theta_0) \times \sin\left[\frac{4\pi r}{\lambda_0}\cos(\phi - m\theta_0)\right], \tag{A20b}$$

where the fictitious magnetic field strength B_0 is

$$B_0 = \frac{9\alpha_1(\omega_0)}{2}E_0^2. \tag{A21}$$

The expansions (A17) and (A20) assure that $V(r,\phi)$, $B_r(r,\phi)$, and $B_\phi(r,\phi)$ are invariant under the transformation $\phi \to \phi' = \phi - m\pi/3$, where m is an integer. Thus, the optical lattice potential $V(\mathbf{r})$ and the fictitious magnetic field $\mathbf{B}(\mathbf{r})$ are invariant under rotations by $\pi/3$ rad around the z axis (see Fig. 1):

$$V\left[U\left(\frac{m\pi}{3}\right)\mathbf{r}\right] = V(\mathbf{r}),$$
$$U\left(\frac{m\pi}{3}\right)\mathbf{B}\left[U\left(\frac{m\pi}{3}\right)\mathbf{r}\right] = \mathbf{B}(\mathbf{r}), \tag{A22}$$

where the rotation matrix $U(\phi)$ is

$$U(\phi) = \begin{pmatrix}\cos\phi & -\sin\phi \\ \sin\phi & \cos\phi\end{pmatrix}.$$

The optical potential (A17) and the fictitious magnetic field (A19) are shown in Figs. 7(a) and 7(b) for $\beta = 1/\sqrt{2}$.

APPENDIX B: ISOTROPIC APPROXIMATION FOR THE SPIN-DEPENDENT OPTICAL LATTICE POTENTIAL

The Fourier transforms for $V(\mathbf{r})$, $B_r(\mathbf{r})$, and $B_\phi(\mathbf{r})$ are

$$V(r,\phi) = \sum_m \tilde{V}_m(r)e^{6im\phi}, \tag{B1}$$
$$B_r(r,\phi) = \sum_m \tilde{B}_{r,m}(r)e^{6im\phi}, \tag{B2}$$
$$B_\phi(r,\phi) = \sum_m \tilde{B}_{\phi,m}(r)e^{6im\phi}, \tag{B3}$$

where m is an integer, and

$$\tilde{\mathcal{F}}_m(r) = \frac{1}{2\pi}\int_0^{2\pi}\mathcal{F}(r,\phi)e^{-6im\phi}d\phi, \quad \mathcal{F} = V, B_r, B_\phi.$$

$V(r,\phi)$, $B_r(r,\phi)$, and $B_\phi(r,\phi)$ are real, and therefore

$$\tilde{\mathcal{F}}_{-m}(r) = \tilde{\mathcal{F}}_m^*(r).$$

Moreover, $V(r,\phi)$ and $B_r(r,\phi)$ are even with respect to the inversion $\phi \to -\phi$, and $B_\phi(r,\phi)$ is odd:

$$V(r,-\phi) = V(r,\phi), \quad B_r(r,-\phi) = B_r(r,\phi),$$
$$B_\phi(r,-\phi) = -B_\phi(r,\phi).$$

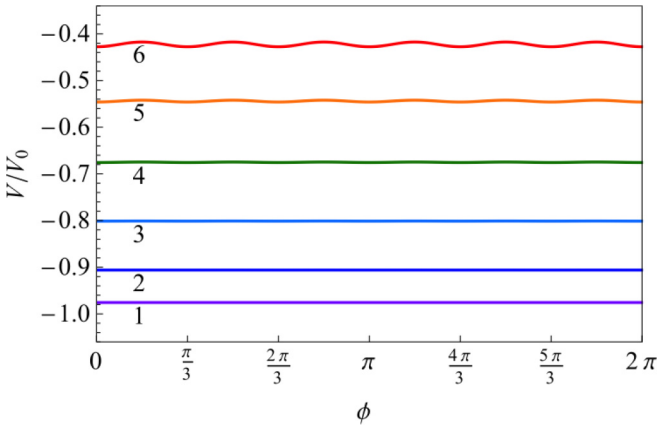

FIG. 8. $V(\mathbf{r})$ (A17) as a function of the polar angle ϕ for $\beta = \frac{1}{\sqrt{2}}$. The purple (1), blue (2), sky blue (3), green (4), orange (5), and red (6) curves denote $r = 0.05\lambda_0$, $0.1\lambda_0$, $0.15\lambda_0$, $0.2\lambda_0$, $0.25\lambda_0$, and $0.3\lambda_0$.

Therefore the Fourier components $\tilde{V}_m$, $\tilde{B}_{r,m}$, and $\tilde{B}_{\phi,m}$ satisfy the properties

$$\tilde{V}_m(r) = \tilde{V}_{-m}(r), \quad \tilde{B}_{r,m}(r) = \tilde{B}_{r,-m}(r),$$
$$\tilde{B}_{\phi,m}(r) = -\tilde{B}_{\phi,-m}(r).$$

1. Isotropic approximation for $V(\mathbf{r})$

Figure 8 shows $V(\mathbf{r})$ as a function of ϕ for $\beta = 1/\sqrt{2}$ and a few values of r. It is clear that for $r < 0.3\lambda_0$ the potential is almost isotropic. Hence, for $r \lesssim 0.3\,\lambda_0$, the optical potential (A17) can be well approximated by the isotropic potential $\tilde{V}(r) \equiv \tilde{V}_0(r)$ given by Eq. (6).

The lowest-order anisotropic correction to the potential in Eq. (B1) is given in terms of the Fourier coefficients:

$$\tilde{V}_1(r) = \tilde{V}_{-1}(r) \approx \frac{V_0}{180}\left(\frac{\pi r}{\lambda_0}\right)^6. \tag{B4}$$

For $r = r_0 = 0.068\,\lambda_0$, where r_0 is the radius where the areal probability density is maximal, $|\tilde{V}_1(r_0)| \approx 5.281 \times 10^{-7}\,V_0$; i.e., it is really small, and therefore the anisotropic corrections can be neglected for the ground and lowest-energy eigenstates.

The isotropic potential $\tilde{V}_0(r)$ is shown in Fig. 10 (blue curve). Clearly, $\tilde{V}_0(r)$ is attractive and increases monotonically with r.

2. Isotropic approximation for B(r)

Figure 9 shows $B_r(\mathbf{r})$ and $B_\phi(\mathbf{r})$ [Eq. (A20)], as functions of ϕ for $\beta = 1/\sqrt{2}$ and several values of r. Clearly, for $r < 0.3\lambda_0$, $B_r(\mathbf{r})$ depends on r, whereas $B_\phi(\mathbf{r})$ oscillates quickly with ϕ, but with very small amplitude. Hence, for $r \lesssim 0.3\lambda_0$, $B_r(\mathbf{r})$ can be approximated by the isotropic function $\tilde{B}(r) \equiv \tilde{B}_{r,0}(r)$:

$$\tilde{B}_{r,0}(r) = \frac{B_0}{3(2I+1)}\left\{J_1\left(\frac{2\pi r}{\lambda_0}\right) + J_1\left(\frac{4\pi r}{\lambda_0}\right) + \sqrt{3}\,J_1\left(\frac{2\sqrt{3}\pi r}{\lambda_0}\right)\right\}, \tag{B5}$$

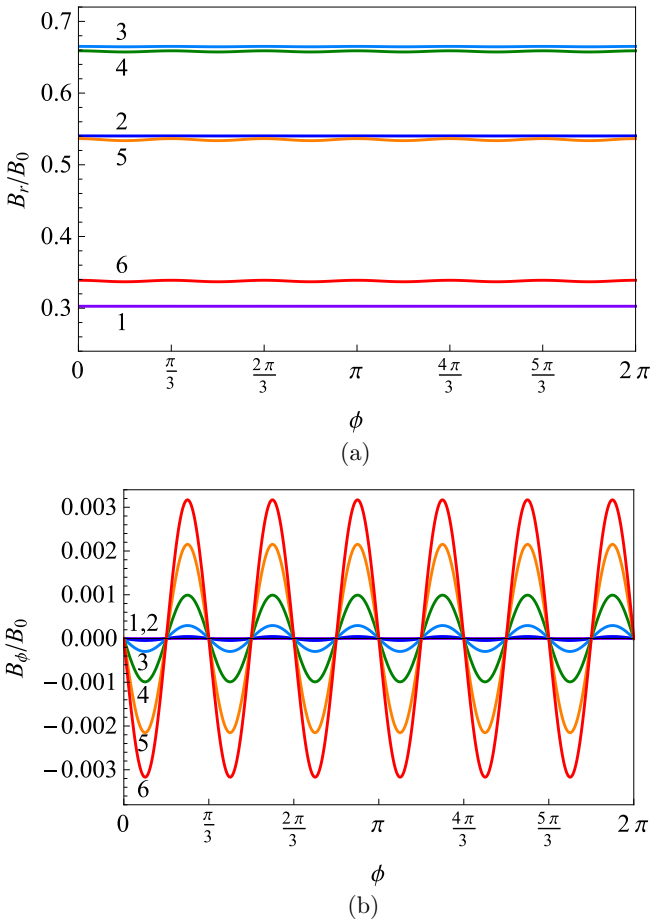

FIG. 9. (a) $B_r(\mathbf{r})$ and (b) $B_\phi(\mathbf{r})$, Eq. (A20), as functions of the polar angle ϕ for $\beta = \frac{1}{\sqrt{2}}$. The purple (1), blue (2), sky blue (3), green (4), orange (5), and red (6) curves denote $r = 0.05\lambda_0$, $0.1\lambda_0$, $0.15\lambda_0$, $0.2\lambda_0$, $0.25\lambda_0$, and $0.3\lambda_0$.

and the isotropic part of $\tilde{B}_{\phi,0}(r)$ vanishes:

$$\tilde{B}_{\phi,0}(r) = 0.$$

The lowest-order anisotropic corrections to $B_r(\mathbf{r})$ and $B_\phi(\mathbf{r})$ in Eqs. (B2) and (B3) are given by the Fourier coefficients

$$\tilde{B}_{r,1}(r) = \tilde{B}_{r,-1}(r) \approx -\frac{B_0}{120(2I+1)}\left(\frac{\pi r}{\lambda_0}\right)^5, \tag{B6}$$

$$\tilde{B}_{\phi,1}(r) = \tilde{B}^*_{\phi,-1}(r) \approx -\frac{iB_0}{120(2I+1)}\left(\frac{\pi r}{\lambda_0}\right)^5. \tag{B7}$$

When $r = r_0 = 0.068\,\lambda_0$, $|\tilde{B}_{r,1}(r_0)| = |\tilde{B}_{\phi,1}(r_0)| \approx 1.236 \times 10^{-6} B_0$ is very small, and the anisotropic part of the magnetic field can be neglected for the ground and lowest excited energy eigenstates.

The isotropic effective radial magnetic field $\tilde{B}(r)$ is shown in Fig. 10 (red curve). Note that $\tilde{B}(0) = 0$. There is a distance $r_B = 0.1722\,\lambda_0$ such that, for $r < r_B$, $\tilde{B}(r)$ increases with increasing r. $\tilde{B}(r)$ reaches its maximum, $\tilde{B}(r_B) = 0.6780\,B_0$, at $r = r_B$, and decreases for $r > r_B$. When $r = r_c = 0.3827\,\lambda_0$, $\tilde{B}(r_c) = 0$, and for $r > r_c$ the fictitious magnetic field reverses its direction from $\hat{\mathbf{r}}$ to $-\hat{\mathbf{r}}$.

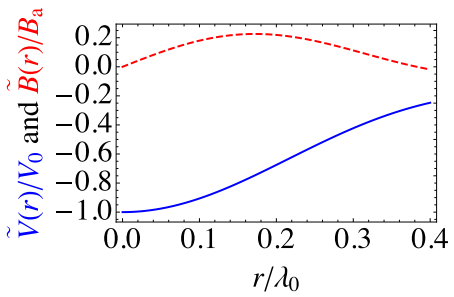

FIG. 10. Spherically symmetric potential $\tilde{V}(r) \equiv \tilde{V}_0(r)$ in units of V_0 and the effective radial magnetic field $\tilde{B}(r) \equiv \tilde{B}_{r,0}(r)$ in units of B_0.

APPENDIX C: PROBABILITY DENSITY FOR $F = 1/2$

At finite temperature T, the probability density to find the atom at position $\mathbf{r}$ in the 2D plane is

$$\rho(r) = \frac{1}{Z}\sum_{n,\zeta} |\Psi_{n,\zeta}(\mathbf{r})|^2 e^{-\beta\epsilon_{n,\zeta}},$$

where

$$Z = \sum_{n,\zeta} e^{-\beta\epsilon_{n,\zeta}},$$

and $\beta = (k_B T)^{-1}$ is proportional to the inverse temperature. At low temperature, where $k_B T$ is much smaller than the orbital excitation energy [see Eq. (11a)], $\rho(r)$ is well approximated by Eq. (12). In the isotropic optical lattice potential approximation, $\rho(r)$ depends only on r and not on ϕ. $\rho(r)$ has a maximum at $r = r_0 = 0.068\,\lambda_0$, and rapidly decays with $|r - r_0|$, as shown in Fig. 3.

APPENDIX D: SEMICLASSICAL DESCRIPTION OF THE QUANTUM ROTOR

When F is large, $F \gg 1$, we can describe the motion of the trapped atoms using a semiclassical approximation. This formulation yields useful insights into the behavior of QRs, and is simple to carry out within the isotropic approximation for the SDOLP [Eqs. (6) and (B5)], which is valid near the minimum of the scalar potential. A power series expansion about the origin yields

$$\tilde{V}_0(r) \approx -V_0 + \frac{\pi^2 V_0 r^2}{\lambda_0^2},$$
$$\tilde{B}_{r,0}(r) \approx \frac{2\pi B_0 r}{(2I+1)\lambda_0}. \tag{D1}$$

In terms of the canonical momentum $\mathbf{p}$ and the unit vector $\mathbf{f} = \mathbf{F}/F$, and using the power series in Eqs. (D1), we arrive at the following Hamilton equations of motion:

$$\dot{\mathbf{r}} = \frac{\mathbf{p}}{M}, \tag{D2a}$$
$$\dot{\mathbf{p}} = -\frac{2\pi^2 V_0}{\lambda_0^2}\mathbf{r} - \frac{2\pi F B_0}{(2I+1)\lambda_0}\mathbf{f}_\parallel, \tag{D2b}$$
$$\dot{\mathbf{f}} = \frac{2\pi B_0}{(2I+1)\hbar\lambda_0}[\mathbf{r}\times\mathbf{f}], \tag{D2c}$$

where $\mathbf{f}_\parallel = f_x\mathbf{e}_x + f_y\mathbf{e}_y$.

It is convenient to use harmonic length and energy units:

$$\text{harmonic length} \quad b_0 = \frac{\lambda_0}{2\pi}\left(\frac{2\mathcal{E}_0}{V_0}\right)^{1/4},$$
$$\text{harmonic energy} \quad \hbar\Omega_h = \sqrt{\frac{\mathcal{E}_0 V_0}{2}},$$

where the recoil energy $\mathcal{E}_0$ is

$$\mathcal{E}_0 = \frac{\hbar^2 q_0^2}{2M} = \frac{2\pi^2\hbar^2}{M\lambda_0^2}. \tag{D3}$$

In this section, we consider ^{40}K atoms which have $I = 4$, $J = 1/2$, and $F = 9/2$ in the ground state. When $V_0 = 100\,\mathcal{E}_0$, $b_0 = 0.05985\,\lambda_0$ and $\hbar\Omega_h = 7.071\,\mathcal{E}_0$. The time-dependent position of the atom $\mathbf{r}(t) = (x(t), y(t))$ and the unit spin vector $\mathbf{f}(t) = (f_x(t), f_y(t))$ are shown in Fig. 11 for $B_0 = 1.8\,V_0$, with the following initial conditions:

$$x(0) = 5\,b_0, \quad y(0) = 0,$$
$$p_x(0) = 0, \quad p_y(0) = -3\hbar/b_0,$$
$$f_x(0) = -0.9975, \quad f_y(0) = 0.05, \quad f_z(0) = 0.05. \tag{D4}$$

The motion of the atom is not periodic, and therefore the trajectory $(x(t), y(t))$ in Fig. 11(a) fills a ring with inner radius $5\,b_0$ and outer radius $6.615\,b_0$, whereas $(f_x(t), f_y(t))$ in Fig. 11(b) fills a ring with inner radius 0.9644 and outer radius 1. For ^{40}K atoms, $\lambda_0 = 766.5$ nm, and $b_0 = 45.87$ nm.

The results of this section cannot be applied to Li atoms because, for the semiclassical approximation to be valid, F must be large.

APPENDIX E: DISTINGUISHING BETWEEN Ω, a, AND $\mathbf{B}_{ex}$

Consider a QR placed in an external magnetic field $\mathbf{B}_{ex}$ in a noninertial frame moving with a linear acceleration $\mathbf{a}$ and rotating with an angular velocity $\boldsymbol{\Omega}$. The three-dimensional Hamiltonian of the QR is

$$H = H_0 + H_z + H_B + H_\Omega + H_a. \tag{E1}$$

Here H_0 is a 2D Hamiltonian for motion of the QR in the x-y plane without an external magnetic field and in an inertial frame; using polar coordinates $\mathbf{r} = (r, \phi)$, $H_0 = -\frac{\hbar^2\nabla^2}{2M} + \tilde{V}(r) - \tilde{B}(r)F_r$. The second term on the right-hand side of Eq. (E1), H_z, is for the motion of the trapped atom in a harmonic potential in the z direction:

$$H_z = -\frac{\hbar^2\partial_z^2}{2M} + \frac{K_z z^2}{2}. \tag{E2}$$

The harmonic oscillator force constant K_z is assumed to be large and the atom is in the ground state of the Hamiltonian (E2). The third term on the right-hand side of Eq. (E1), H_B, is the Zeeman interaction between the QR and the external magnetic field $\mathbf{B}_{ex}$, $H_B = -\frac{g\mu_B}{2I+1}\mathbf{F}\cdot\mathbf{B}_{ex}$. The fourth term, H_Ω, is due to the fictitious force in a rotating frame of reference, $H_\Omega = \hbar\boldsymbol{\mathcal{L}}\cdot\boldsymbol{\Omega}$, where $\boldsymbol{\mathcal{L}} = \mathbf{F} + \boldsymbol{\ell}$, and $\boldsymbol{\ell}$ is the orbital angular momentum of the atom around minimum points of $\tilde{V}(r)$. The fifth term, H_a, is due to the fictitious force appearing in a noninertial frame moving with linear acceleration $\mathbf{a}$, $H_a = M\mathbf{a}\cdot\mathbf{r}$.

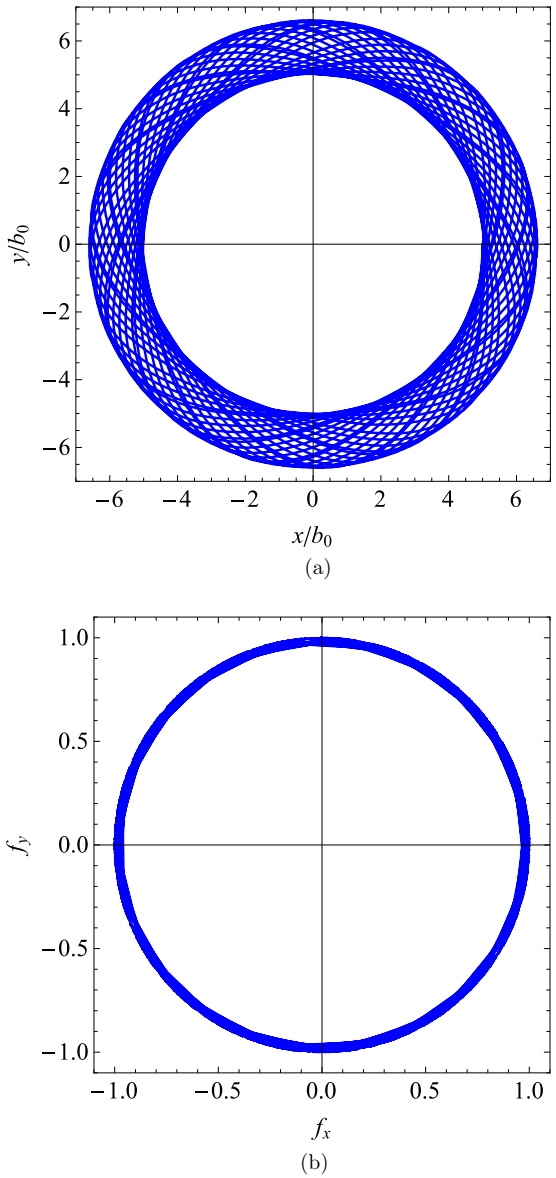

FIG. 11. (a) Position of the trapped atom $\mathbf{r}(t) = (x(t), y(t))$ and (b) the unit vector $\mathbf{f}(t) = (f_x(t), f_y(t))$ parallel to the atomic orbital momentum. Here, we have taken $B_0 = 1.8V_0$ and initial conditions (initial position, momentum, and the direction of the total atomic angular momentum), $\mathbf{f}(t) = \mathbf{F}(t)/|\mathbf{f}(t)|$, given by Eq. (D4).

We shall calculate energy levels of $H_0 + H_z$ in the inertial frame, and then apply first-order perturbation theory in $\mathbf{B}_{\rm ex}$, $\mathbf{\Omega}$, and $\mathbf{a}$, to find the corrections to the energies of the QR.

1. Matrix elements of H_B

Matrix elements of F_x, F_y, and F_z are

$$\langle n,\zeta|F_x|n,\zeta'\rangle = \frac{1}{2}\beta^{\parallel}_{n,\zeta}(\delta_{\zeta,\zeta'+1} + \delta_{\zeta,\zeta'-1}),$$

$$\langle n,\zeta|F_y|n,\zeta'\rangle = -\frac{i}{2}\beta^{\parallel}_{n,\zeta}(\delta_{\zeta,\zeta'+1} - \delta_{\zeta,\zeta'-1}),$$

$$\langle n,\zeta|F_z|n,\zeta'\rangle = \beta^{z}_{n,\zeta}\delta_{\zeta,\zeta'},$$

where $\langle z,\mathbf{r}|n,\zeta\rangle = \tilde{\psi}_0(z)\Psi_{n,\zeta}(\mathbf{r})$, and

$$\beta^{\parallel}_{n,\zeta} = \frac{1}{2}\int\left\{\psi^2_{n,\zeta,1/2}(r) - \psi^2_{n,\zeta,-1/2}(r)\right\}dr, \tag{E3}$$

$$\beta^{z}_{n,\zeta} = \int \psi_{n,\zeta,1/2}(r)\psi_{n,\zeta,-1/2}(r)\,dr. \tag{E4}$$

Note the following symmetries:

$$\beta^{\parallel}_{n,-\zeta} = \beta^{\parallel}_{n,\zeta}, \quad \beta^{z}_{n,-\zeta} = -\beta^{z}_{n,\zeta}.$$

These follow from the wave-function symmetries $\psi_{n,-\zeta,1/2}(r) = \psi_{n,\zeta,1/2}(r)$ and $\psi_{n,-\zeta,-1/2}(r) = -\psi_{n,\zeta,-1/2}(r)$. The matrix elements of H_B are

$$\langle n,\zeta|H_B|n,\zeta'\rangle = -\frac{g\mu_B}{2I+1}\left\{\zeta B_z\beta^{z}_{n,\zeta}\delta_{\zeta,\zeta'} + \frac{\beta^{\parallel}_{n,\zeta}}{2}\left[B^{+}\delta_{\zeta,\zeta'-1} + B^{-}\delta_{\zeta,\zeta'+1}\right]\right\}, \tag{E5}$$

where $B^{\pm} = B_x \pm iB_y$.

2. Matrix elements of H_Ω

Matrix elements of the operator $\boldsymbol{\mathcal{L}}$ are

$$\langle n,\zeta|\mathcal{L}_x|n,\zeta'\rangle = \langle n,\zeta|\mathcal{L}_y|n,\zeta'\rangle = 0,$$
$$\langle n,\zeta|\mathcal{L}_z|n,\zeta'\rangle = \zeta\Omega_z.$$

The matrix elements of $\mathcal{L}_x$ and $\mathcal{L}_y$ vanish since the wave function $\tilde{\psi}_0(z)$ is even with respect to the inversion $z \to -z$, whereas $\mathcal{L}_x$ and $\mathcal{L}_y$ are odd. Hence, nonvanishing matrix elements of H_Ω are

$$\langle n,\zeta|H_\Omega|n,\zeta'\rangle = \hbar\zeta\Omega_z\delta_{\zeta,\zeta'}. \tag{E6}$$

3. Matrix elements of H_a

Matrix elements of the position operator $\mathbf{r}$ are

$$\langle n,\zeta|x|n,\zeta'\rangle = \frac{1}{2}\varrho^{\parallel}_{n,\zeta}(\delta_{\zeta,\zeta'+1} + \delta_{\zeta,\zeta'-1}),$$

$$\langle n,\zeta|y|n,\zeta'\rangle = -\frac{i}{2}\varrho^{\parallel}_{n,\zeta}(\delta_{\zeta,\zeta'+1} - \delta_{\zeta,\zeta'-1}),$$

$$\langle n,\zeta|z|n,\zeta'\rangle = 0,$$

where

$$\varrho^{\parallel}_{n,\zeta} = \int\left\{\psi^2_{n,\zeta,1/2}(r) + \psi^2_{n,\zeta,-1/2}(r)\right\}rdr. \tag{E7}$$

Note the symmetry $\varrho^{\parallel}_{n,-\zeta} = \varrho^{\parallel}_{n,\zeta}$. The matrix elements of H_a are

$$\langle n,\zeta|H_a|n,\zeta'\rangle = \frac{M\varrho^{\parallel}_{n,\zeta}}{2}\left[a^{+}\delta_{\zeta,\zeta'-1} + a^{-}\delta_{\zeta,\zeta'+1}\right], \tag{E8}$$

where $a^{\pm} = a_x \pm ia_y$.

4. First-order corrections to the energies

In order to find the first-order corrections to the energies of the QR due to **B**, **Ω**, and **a**, we apply degenerate perturbation theory. First-order corrections to the energies of the quantum states with $\zeta = \pm 1/2$ are

$$\varepsilon^{(1)}_{n,\pm 1/2}(\mathbf{B}, \Omega_z, a_\parallel) = \pm\frac{1}{2}\Bigg[\left(\frac{g\mu_B\beta^z_{n,1/2}}{2I+1}B_z + \hbar\Omega_z\right)^2 + |\beta^\parallel_{n,1/2}B^+ + M\varrho^\parallel_{n,1/2}a^+|^2\Bigg]^{1/2}. \quad \text{(E9)}$$

Corrections to the energies of the quantum states with $\pm\zeta$ (where $\zeta = 3/2, 5/2, 7/2, \ldots$) are

$$\varepsilon^{(1)}_{n,\pm\zeta}(\mathbf{B}, \Omega_z, a_\parallel) = \pm\zeta\left(\frac{g\mu_B\beta^z_{n,\zeta}}{2I+1}B_z + \hbar\Omega_z\right). \quad \text{(E10)}$$

5. Raman spectroscopy considerations for distinguishing between various sensors

We propose to use Raman spectroscopy to measure **B**, **Ω**, and **a** by applying radio-frequency electromagnetic waves to the QR with pump and Stokes frequencies ($\omega_p > \omega_s$) that are far-off-resonance from the $F = 3/2$ atomic hyperfine state. In Sec. III A we discussed the Raman transition $|0, 1/2\rangle \leftrightarrow |0, -1/2\rangle$ and the use of the Ramsey separated oscillating fields method to verify the Raman resonance condition $\omega \equiv \omega_p - \omega_s = \Delta_{\rm QR}$. In order to determine **Ω**, **a**, and $\mathbf{B}_{\rm ex}$, we will need to consider the Raman transitions $|0, 1/2\rangle \leftrightarrow |0, -1/2\rangle$, $|0, 3/2\rangle \leftrightarrow |0, 5/2\rangle$, and $|0, -3/2\rangle \leftrightarrow |0, -5/2\rangle$, which have transition frequencies $\Delta_0 \equiv \Delta_{\rm QR}$, Δ_+, and Δ_-, respectively:

$$\Delta_0 = \frac{1}{\hbar}\left[\varepsilon^{(1)}_{0,1/2}(\mathbf{B}, \Omega_z, a_\parallel) - \varepsilon^{(1)}_{0,-1/2}(\mathbf{B}, \Omega_z, a_\parallel)\right],$$

$$\Delta_\pm = \frac{1}{\hbar}\left[\epsilon_{0,5/2} - \epsilon_{0,3/2} + \varepsilon^{(1)}_{0,\pm 5/2}(\mathbf{B}, \Omega_z, a_\parallel) - \varepsilon^{(1)}_{0,\pm 3/2}(\mathbf{B}, \Omega_z, a_\parallel)\right].$$

Note that when $\mathbf{B}_{\rm ex} = 0$, $\mathbf{\Omega} = 0$, and $\mathbf{a} = 0$ then

$$\Delta^{(0)}_+ = \Delta^{(0)}_- = \frac{1}{\hbar}(\epsilon_{0,5/2} - \epsilon_{0,3/2}).$$

We are interested in the splitting $\Delta_1 = \Delta_+ - \Delta_-$ due to $\mathbf{B}_{\rm ex}$, **Ω**, and **a**. Using Eqs. (E9) and (E10), we get

$$\Delta_0\left(B_x, B_y, B_z, \Omega_z, a_x, a_y; \varrho^\parallel_{0,1/2}, \beta^\parallel_{0,1/2}, \beta^z_{0,1/2}\right) = \frac{1}{\hbar}\Bigg[\left(\frac{g\mu_B\beta^z_{0,1/2}}{2I+1}B_z + \hbar\Omega_z\right)^2 + \left(\frac{g\mu_B\beta^\parallel_{0,1/2}}{2I+1}B_x + M\varrho^\parallel_{0,1/2}a_x\right)^2 + \left(\frac{g\mu_B\beta^\parallel_{0,1/2}}{2I+1}B_y + M\varrho^\parallel_{0,1/2}a_y\right)^2\Bigg]^{1/2}, \quad \text{(E11)}$$

$$\Delta_1\left(B_z, \Omega_z; \beta^z_{0,3/2}, \beta^z_{0,5/2}\right) = \frac{1}{\hbar}\left\{2\hbar\Omega_z + \frac{g\mu_B}{2I+1}\left(5\beta^z_{0,5/2} - 3\beta^z_{0,3/2}\right)B_z\right\}. \quad \text{(E12)}$$

Nine measurements need to be made to allow determination of the nine unknowns: B_z, B_y, B_z, Ω_x, Ω_y, Ω_z, a_x, a_y, and a_z. In order to find the nine unknowns, nine measurements are required. In particular, measurements must be carried out with the QR placed in x-y, y-z, and z-x optical lattices. Moreover, measurements of Δ_1 must be made with two different laser intensities, e.g., $(V_0, B_0) = (100\,\mathcal{E}_0, 180\,\mathcal{E}_0)$ and $(50\,\mathcal{E}_0, 90\,\mathcal{E}_0)$. In other words, we consider $(V_0, B_0) = (10\mathcal{N}\mathcal{E}_0, 18\mathcal{N}\mathcal{E}_0)$, where the dimensionless parameter $\mathcal{N} = 5$ and 10 specifies the laser intensity. Furthermore, measurements of Δ_0 must be made with $V_0 = 100\,\mathcal{E}_0$ and $B_0 = 180\,\mathcal{E}_0$.

The numerical solution of the Schrödinger equation (9) for different values of $\mathcal{N}$ yields the following results for the integrals $\beta^z_{0,1/2}(\mathcal{N})$, $\beta^z_{0,3/2}(\mathcal{N})$, $\beta^z_{0,5/2}(\mathcal{N})$, $\beta^\parallel_{0,1/2}(\mathcal{N})$, and $\varrho^\parallel_{0,1/2}(\mathcal{N})$. The values of $\beta^z_{0,3/2}(\mathcal{N})$ and $\beta^z_{0,5/2}(\mathcal{N})$ for $\mathcal{N} = 5$ and 10 are (see Figs. 12(d) and 12(e))

$$\beta^z_{0,3/2}(5) = 0.161531, \quad \beta^z_{0,3/2}(10) = 0.117236,$$

$$\beta^z_{0,5/2}(5) = 0.154678, \quad \beta^z_{0,5/2}(10) = 0.111702.$$

The values of $\beta^z_{0,1/2}(10)$, $\beta^\parallel_{0,1/2}(10)$, and $\varrho^\parallel_{0,1/2}(10)$ for $\mathcal{N} = 10$ are (see Figs. 12(a), 12(b) and 12(c))

$$\beta^z_{0,1/2}(10) = 0.107807, \quad \beta^\parallel_{0,1/2}(10) = 0.478494,$$

$$\varrho^\parallel_{0,1/2}(10) = 0.0986575\lambda_0.$$

6. Determining $\mathbf{B}_{\rm ex}$, Ω, and a

With the optical lattice in the x-y plane, measurements can be made of $\Delta_{1,xy}(\mathcal{N})$ for $\mathcal{N} = 5$ and 10. Two equations (one for $\mathcal{N} = 5$ and one for $\mathcal{N} = 10$) are thereby obtained from

$$\frac{g\mu_B B_z}{\hbar(2I+1)}\left[5\beta^z_{0,5/2}(\mathcal{N}) - 3\beta^z_{0,3/2}(\mathcal{N})\right] + 2\Omega_z = \Delta_{1,xy}(\mathcal{N}). \quad \text{(E13)}$$

The solution of these equations is

$$B_z = \frac{2I+1}{g\mu_B}\frac{\hbar[\Delta_{1,xy}(10) - \Delta_{1,xy}(5)]}{\tilde\beta(10) - \tilde\beta(5)}, \quad \text{(E14)}$$

$$\Omega_z = \frac{\tilde\beta(10)\,\Delta_{1,xy}(5) - \tilde\beta(5)\,\Delta_{1,xy}(10)}{\tilde\beta(10) - \tilde\beta(5)}, \quad \text{(E15)}$$

where

$$\tilde\beta(\mathcal{N}) = 5\beta^z_{0,5/2}(\mathcal{N}) - 3\beta^z_{0,3/2}(\mathcal{N}).$$

With the optical lattice arranged in y-z and z-x planes, measurements can be made of $\Delta_{1,yz}(\mathcal{N})$ and $\Delta_{1,zx}(\mathcal{N})$ for $\mathcal{N} = 5$ and 10. These measurements allow us to find B_x, B_y, Ω_x, and Ω_y:

$$B_x = \frac{2I+1}{g\mu_B}\frac{\hbar[\Delta_{1,yz}(10) - \Delta_{1,yz}(5)]}{\tilde\beta(10) - \tilde\beta(5)}, \quad \text{(E16)}$$

$$B_y = \frac{2I+1}{g\mu_B}\frac{\hbar[\Delta_{1,zx}(10) - \Delta_{1,zx}(5)]}{\tilde\beta(10) - \tilde\beta(5)}, \quad \text{(E17)}$$

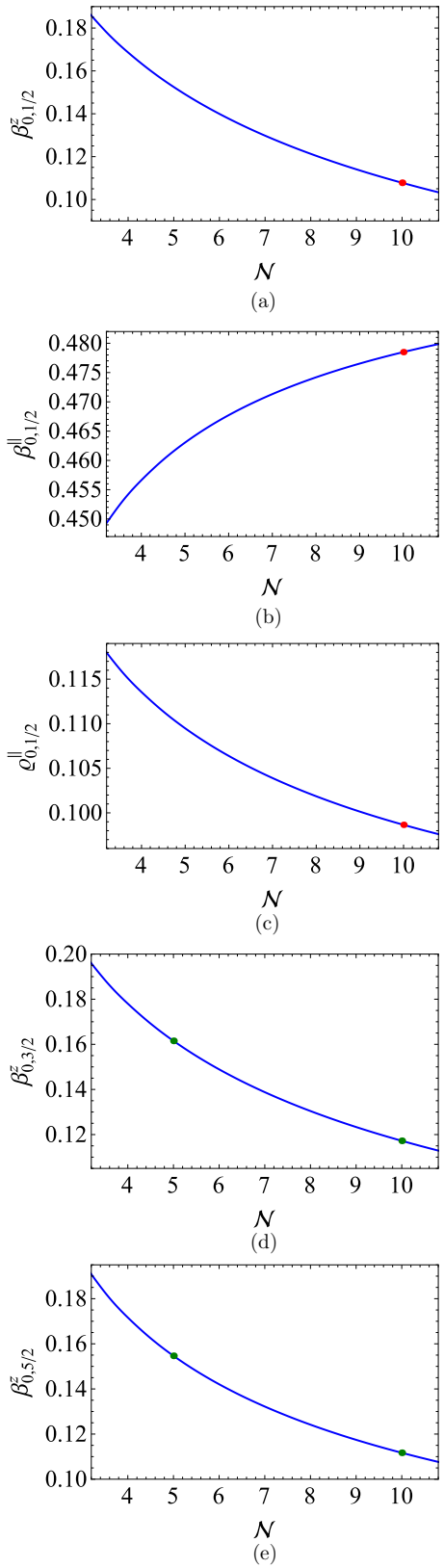

FIG. 12. (a) $\beta^z_{0,1/2}$ (E4), (b) $\beta^{\parallel}_{0,1/2}$ (E3), (c) $\varrho^{\parallel}_{0,1/2}$ (E7), (d) $\beta^z_{0,3/2}$ (E4), and (e) $\beta^z_{0,5/2}$ (E4) as functions of $\mathcal{N}$. The red dots denote the values of $\beta^z_{0,1/2}$, $\beta^{\parallel}_{0,1/2}$, and $\varrho^{\parallel}_{0,1/2}$ for $\mathcal{N}=10$, and the green dots denote the values of $\beta^z_{0,3/2}$ and $\beta^z_{0,5/2}$ for $\mathcal{N}=5$ and 10.

$$\Omega_x = \frac{\tilde{\beta}(10)\,\Delta_{1,yz}(5) - \tilde{\beta}(5)\,\Delta_{1,yz}(10)}{\tilde{\beta}(10) - \tilde{\beta}(5)}, \tag{E18}$$

$$\Omega_y = \frac{\tilde{\beta}(10)\,\Delta_{1,yz}(5) - \tilde{\beta}(5)\,\Delta_{1,yz}(10)}{\tilde{\beta}(10) - \tilde{\beta}(5)}. \tag{E19}$$

With the optical lattice arranged in the x-y, y-z, and z-x planes, measurements can be made of $\Delta_{0,xy}$, $\Delta_{0,yz}$, and $\Delta_{0,zx}$ for $\mathcal{N}=10$. Three equations are thereby obtained:

$$\left(\frac{g\mu_B\beta^{\parallel}_{0,1/2}}{2I+1}B_\alpha + M\varrho^{\parallel}_{0,1/2}a_\alpha\right)^2 + \left(\frac{g\mu_B\beta^{\parallel}_{0,1/2}}{2I+1}B_{\alpha'} + M\varrho^{\parallel}_{0,1/2}a_{\alpha'}\right)^2 + \left(\frac{g\mu_B\beta^{z}_{0,1/2}}{2I+1}B_{\alpha''} + \hbar\Omega_{\alpha''}\right)^2 = \hbar^2\Delta^2_{0,\alpha\alpha'}, \tag{E20}$$

where $(\alpha,\alpha',\alpha'')=(x,y,z)$, (y,z,x), and (z,x,y). Here B_α are given by Eqs. (E14), (E16), and (E17) for $\alpha=z,x,y$, whereas Ω_α are given by Eqs. (E15), (E18), and (E19). The solution of Eq. (E20) is

$$a_x = \frac{1}{M\varrho^{\parallel}_{0,1/2}}\left\{\frac{1}{2}\sqrt{A_{x,y}+A_{z,x}-A_{y,z}} - \frac{g\mu_B\beta^{\parallel}_{0,1/2}}{2I+1}B_x\right\}, \tag{E21}$$

$$a_y = \frac{1}{M\varrho^{\parallel}_{0,1/2}}\left\{\frac{1}{2}\sqrt{A_{y,z}+A_{x,y}-A_{z,x}} - \frac{g\mu_B\beta^{\parallel}_{0,1/2}}{2I+1}B_y\right\}, \tag{E22}$$

$$a_z = \frac{1}{M\varrho^{\parallel}_{0,1/2}}\left\{\frac{1}{2}\sqrt{A_{z,x}+A_{y,z}-A_{x,y}} - \frac{g\mu_B\beta^{\parallel}_{0,1/2}}{2I+1}B_z\right\}, \tag{E23}$$

where

$$A_{\alpha,\alpha'} = \hbar^2\Delta^2_{0,\alpha\alpha'} - \left(\frac{g\mu_B\beta^{z}_{0,1/2}}{2I+1}B_{\alpha''} + \hbar\Omega_{\alpha''}\right)^2,$$

and $(\alpha,\alpha',\alpha'')=(x,y,z)$, (y,z,x) and (z,x,y).

As already discussed in Sec. III A in connection with the far-off-resonance Raman transition $|0,1/2\rangle \leftrightarrow |0,-1/2\rangle$, to determine the Raman resonance condition $\omega_p-\omega_s=\Delta$ in *all* the far-off-resonance Raman processes considered in this section, ($|0,1/2\rangle \leftrightarrow |0,-1/2\rangle$, $|0,3/2\rangle \leftrightarrow |0,5/2\rangle$, and $|0,-3/2\rangle \leftrightarrow |0,-5/2\rangle$), one can employ the Ramsey time-separated oscillating field method [24] with Raman pulses [25].

[1] S. Sachdev, *Quantum Phase Transitions*, 2nd ed. (Cambridge University, Cambridge, England, 2011), pp. 12–14.

[2] https://en.wikipedia.org/wiki/Quantum_rotor_model.

[3] L. Allen, M. W. Beijersbergen, R. J. C. Spreeuw, and J. P. Woerdman, Phys. Rev. A **45**, 8185 (1992).

[4] M. A. Clifford, J. Arlt, J. Courtial, and K. Dholakia, Opt. Commun. **156**, 300 (1998).

[5] L. Amico, A. Osterloh, and F. Cataliotti, Phys. Rev. Lett. **95**, 063201 (2005).

[6] A. Kumar, N. Anderson, W. D. Phillips, S. Eckel, G. K. Campbell and S. Stringari, New J. Phys. **18**, 025001 (2016).

[7] Y.-J. Lin, K. Jimnez-Garca, and I. B. Spielman, Nature (London) **471**, 83 (2011).

[8] A. M. Dudarev, R. B. Diener, I. Carusotto, and Q. Niu, Phys. Rev. Lett. **92**, 153005 (2004).

[9] F. Le Kien, P. Schneeweiss and A. Rauschenbeutel, Eur. Phys. J. D **67**, 92 (2013).

[10] V. Galitski and I. B. Spielman, Nature (London) **494**, 49 (2013).

[11] G. Juzeliunas, J. Ruseckas, and J. Dalibard, Phys. Rev. A **81**, 053403 (2010).

[12] X.-J. Liu, K. T. Law, and T. K. Ng, Phys. Rev. Lett. **112**, 086401 (2014).

[13] C. Zhang, S. Tewari, R. M. Lutchyn, and S. Das Sarma, Phys. Rev. Lett. **101**, 160401 (2008).

[14] It is also of interest to explore SDOLP with other symmetries.

[15] Strictly speaking, when atoms have $J = 1/2$ and $F > 1/2$, the high-order terms within perturbation theory in powers of the electric field generate tensor interactions (quadrupole, octupole, etc.) of the atoms with the SDOLP. However, within second-order perturbation theory (as used here in our paper), just scalar and vector potentials appear for atoms with $J = 1/2$ and any F (even $F > 1/2$).

[16] C. Cohen-Tannoudji and J. Dupont-Roc, Phys. Rev. A **5**, 968 (1972).

[17] J. H. Becher, S. Baier, K. Aikawa, M. Lepers, J.-F. Wyart, O. Dulieu, and F. Ferlaino, Phys. Rev. A **97**, 012509 (2018).

[18] S. G. Karshenboim and V. G. Ivanov, Phys. Lett. B **524**, 259 (2002).

[19] One could do a full band-structure calculation, but our interest is in the lowest-energy states with negligible well to well tunneling and wave functions localized at small r, hence the 2D isotropic approximation is sufficient.

[20] C. Weitenberg, M. Endres, J. F. Sherson, M. Cheneau, P. Schauß, T. Fukuhara, I. Bloch, and S. Kuhr, Nature (London) **471**, 319 (2011).

[21] C. Cohen-Tannoudji and S. Reynaud, J. Phys. B: Atom. Molec. Phys. **10**, 345 (1977).

[22] V. V. Sokolov and V. G. Zelevinsky, Ann. Phys. (NY) **216**, 323 (1992).

[23] V. B. Berestetskii, E. M. Lifshitz, and L. P. Pitaevskii, *Relativistic Quantum Theory*, 2nd ed., Course of Theoretical Physics Vol. 4 (Pergamon, New York, 1982), pp. 153–155.

[24] N. F. Ramsey, Phys. Rev. **78**, 695 (1950).

[25] T. Zanon-Willette, S. Almonacil, E. de Clercq, A. D. Ludlow, and E. Arimondo, Phys. Rev. A **90**, 053427 (2014).

[26] D. Budker and M. Romalis, Nat. Phys. **3**, 227 (2007).

[27] L. Viverit, C. Menotti, T. Calarco, and A. Smerzi, Phys. Rev. Lett. **93**, 110401 (2004).

[28] I. Bloch, J. Dalibard, and W. Zwerger, Rev. Mod. Phys. **80**, 885 (2008).

[29] L. J. Radziemski, R. Engleman, Jr., and J. W. Brault, Phys. Rev. A **52**, 4462 (1995).

[30] H. Al-Taiy, N. Wenzel, S. Preußler, J. Klinger, and T. Schneider, Opt. Lett. **39**, 5826 (2014).

[31] D. Budker and D. F. J. Kimball, *Optical Magnetometry* (Cambridge University, Cambridge, England, 2013), pp. 4–5.